Fluid Phase Equilibria 582 (2024) 114102

Contents lists available at ScienceDirect

Fluid Phase Equilibria

journal homepage: www.journals.elsevier.com/fluid-phase-equilibria

Hydrophobic interactions described using hetero-segmented PC-SAFT: 1. Alcohol/water mixtures

Marius Rother, Gabriele Sadowski *

Laboratory of Thermodynamics, TU Dortmund, Emil-Figge-Str. 70, D-44227 Dortmund, Germany

ARTICLE INFO

Keywords:
PC-SAFT
Group contribution method
Water–hydrocarbon mixtures
Hydrophobic effect

ABSTRACT

The hydrophobic effect plays a central role in aqueous systems containing molecules with hydrophobic moieties. Despite the relevance of this effect for chemical processes or pharmaceutical applications, modeling remains challenging even using molecular-based models such as different versions of the Statistical Associating Fluid Theory. This work shows the feasibility of hetero-segmented PC-SAFT for this purpose. This model was used as a group contribution method to build molecules from different functional groups, namely from CH_2, CH_3, and CH_2OH groups. Saturated-liquid densities and vapor pressures of n-alkanes and n-alcohols as well as binary mixtures of these molecules were accurately described by this approach. The description of aqueous mixtures containing n-alkanes and n-alcohols was improved compared to state-of-the-art modeling by explicitly accounting for intermolecular interactions resulting in the hydrophobic effect. The so-obtained framework describes the two liquid–liquid equilibrium phases in mixtures of n-alkanes or n-alcohols with water equally well using a single set of transferable parameters. The model was also validated for vapor–liquid equilibria, solid–liquid equilibria, infinite-dilution properties, as well as octanol/water partition coefficients and showed quantitative agreement with experimental data.

1. Introduction

Despite their importance for industry and pharmaceutical applications, describing aqueous systems that contain hydrophobic components has long been a challenging task in thermodynamic modeling [1]. This challenge is caused by the complex intermolecular interactions between water and hydrophobic molecules resulting in the so-called hydrophobic effect. This effect describes the energetically unfavorable constellation, that hydrophobic molecules or functional moieties are dispersed in an aqueous solution [2]. To minimize its energy, the system reduces the proportion of water molecules in contact with the hydrophobic molecules, either microscopically by clustering of the hydrophobic molecules, also known as hydrophobic association [3,4] or macroscopically by liquid–liquid demixing [2]. The latter is a well-known observation in aqueous mixtures with long-chain hydrocarbons having a broad miscibility gap with a pronounced minimum in the aqueous solubility at approximately 300 K [5].

Although up today there is no scientific consensus about the molecular origin, it is widely assumed that this effect is caused by the ability of water molecules to form persistent and flexible networks based on hydrogen bonds throughout the liquid phase. If a hydrophobic solute is dispersed in such an environment, this local water network is distorted due to a complex interplay of entropic and enthalpic driving forces which change with temperature, solute size, and shape [2,4,6–8]. This becomes particularly important for highly functionalized solutes, where the phase behavior in aqueous systems results from a sensitive balance between hydrophilic and hydrophobic interactions. Especially for pharmaceutical applications this balance is of great relevance given the omnipresence of water.

Several attempts have been made to model these kinds of systems. Within this course, it is often convenient to initiate research with simple systems, such as mixtures of water and n-alkanes and mixtures of water and n-alcohols, before progressing to more complex molecules. In many scientific contributions, it has been shown that the direct consideration of all manifestations of molecular association, including self-association and solvation phenomena, is a prerequisite for successfully modeling these systems [9–11]. A comprehensive review on the application of molecular-based models to explicitly consider molecular association for aqueous solutions containing hydrophobic molecules, such as different incarnations of the Statistical Associating Fluid Theory (SAFT), can be found in [1]. Briefly, the main challenge is to correctly depict the

* Corresponding author.
E-mail address: gabriele.sadowski@tu-dortmund.de (G. Sadowski).

https://doi.org/10.1016/j.fluid.2024.114102
Received 29 February 2024; Received in revised form 5 April 2024; Accepted 8 April 2024
Available online 9 April 2024

List of symbols

Roman

a	Molar Helmholtz energy (J mole^{-1})
$AARD$	Average absolute relative deviation (-)
C_N	Number of carbon atoms (-)
c_p	Isobaric heat capacity (J mole^{-1} K^{-1})
g_{ij}^{HS}	Hard-sphere radial distribution function at contact (-)
h	Molar enthalpy (J mole^{-1})
C_{ij}	Henry constant of solute i in solvent j (Pa)
k_B	Boltzmann constant (J K^{-1})
k_{ij}	Binary interaction parameter for dispersion energy (-)
k_{ij}^{HB}	Binary interaction parameter for association energy (-)
K_{OW}	Octanol/water partition coefficient (-)
l_{ij}	Binary interaction parameter for segment diameter (-)
l_{ij}^{HB}	Binary interaction parameter for association volume (-)
m_i	Number of segments of component i (-)
mM_i^{-1}	Number of segments per molar mass (mole g^{-1})
N_i^{Assoc}	Number of association sites component I (-)
N_D	Number of data points (-)
N_C	Number of components (-)
p	Pressure (Pa)
R	Universal gas constant (J mole^{-1} K^{-1})
T	Temperature (K)
u	Potential energy (J)
x_i	Mole fraction component i (-)
Z	Compressibility factor (-)

Greek

γ_i	Activity coefficient of component i (-)
Δ	Difference
$\Delta^{A_iB_j}$	Association strength between groups i and j (Å^3)
$\varepsilon^{A_iB_j}$	Association energy between groups i and j (J)
$\kappa^{A_iB_j}$	Association volume between groups i and j (J)
ρ	Molar density (mole m^{-3})
σ	Segment diameter (Å)
φ_i	Fugacity coefficient of component i (-)

Subscript

$0i$	Pure-component i
i,j	Components/groups

Superscript

aq	Aqueous phase
assoc	Association
disp	Dispersion
E	Excess
hc	Hard chain
LV	Liquid−vapor
org	Organic phase
res	Residual
SL	Solid-liquid

Abbreviation

BIP	Binary interaction parameter
C_N	n-alkane with N carbon atoms
C_NOH	n-alcohol with N carbon atoms
GC	Group contribution
LLE	Liquid–liquid equilibrium
PE	Polyethylene
PC-SAFT	Perturbed-Chain Statistical Associating Fluid Theory
SAFT	Statistical Associating Fluid Theory
SLE	Solid–liquid equilibrium
VLE	Vapor–liquid equilibrium

asymmetry between the mutual solubilities of water and the hydrophobic solute as well as the solubility minimum of the hydrophobic solute in the aqueous phase. Furthermore, the authors of the review emphasized that a significant influence on success stems from the choice of parameters for each compound, in particular for water [1].

This was later confirmed by Haarmann et al. [12], who proved that the Perturbed-Chain SAFT (PC-SAFT) [13,14] is able to accurately model the mutual solubilities in n-alkane/water mixtures by using a 4C parameter set for water and a temperature-dependent interaction parameter for the dispersive energy. Additionally, they found that the different interaction parameters of the single water/n-alkane systems follow a well-defined relationship indicating a physically-sound foundation of this approach [12]. A similar strategy has been followed by Ahmed et al. [15], who generated new water parameters by simultaneously fitting them to pure-component water properties and to data on binary systems with n-alkanes. They accomplished very good results for modeling the mutual aqueous solubilities for a number of hydrophobic components, including long-chain n-alkanes and n-alcohols, using a homo-segmented group contribution (GC) method for PC-SAFT. Similar success was achieved by Hutacharoen et al. [16] for fluid-phase equilibria of aqueous mixtures of long-chain n-alkanes and n-alcohols applying the SAFT-γ Mie GC method but with independently adapted water parameters. The success of the two approaches is particularly characterized by the fact that all mixtures have been described using a unique set of transferable parameters. This constitutes a challenging test for GC methods since the model must combine hydrophobic and hydrophilic groups in a way that the correct balance of the different intermolecular interactions is obtained. However, the two approaches fail to capture the solubility minimum of the hydrophobic component in the aqueous phase.

This was resolved by NguyenHuynh [17] using a modified GC PC-SAFT approach originally developed by Passarello and de Hemptinne [18–23]. He captured this solubility minimum by applying a temperature-dependent interaction parameter, similar to the work of Haarmann et al. [12]. He achieved extraordinary results for aqueous mixtures containing n-alkanes, 1-alkenes, and cycloalkanes, again using only a single set of parameters for a whole set of homologues. However, long-chain n-alcohols were not considered.

In a follow-up work, this was attained by Haarmann et al. [24] employing a hetero-segmented PC-SAFT method. They extended the modeling to aqueous solutions containing long-chain self-associating components, such as n-alcohols, n-amines, and n-alkyl carboxylic acids. For this purpose, they modeled the n-alkylic residue with the parameter set of pure n-alkanes, whereas the parameters of the head were separately determined. In this way, they were able to fully reuse the results describing n-alkanes with water [12]. Remarkably, the model captured the temperature minimum of the long-chain n-alcohols solubility in the aqueous phase and also the decreasing aqueous solubility with increasing chain length in a fully predictive manner.

In a more recent work, Tan et al. [25] further improved the description of aqueous systems containing small hydrocarbons by allowing cross-association between water and hydrocarbon molecules. They argued that the model's failure to describe all equilibrium phases simultaneously is caused by the common approach assuming that water and hydrocarbon molecules exclusively interact through non-polar van der Waals type forces. They referred to independent researches [26–29] also indicating induced polar interactions between hydrophobic molecules, such as n-alkanes and water. It was also concluded that these polar

interactions are crucial to correctly predict the equilibrium water content in n-alkanes. To account for these interactions, Tan et al. [25] employed the framework of induced association proposed by Kleiner and Sadowski [30] and showed, that this enables PC-SAFT to describe all equilibrium phases in mixtures of water and small alkanes equally well.

Our future focus is devoted to model aqueous surfactant systems. These systems serve as prototypes for aqueous solutions which are governed by a delicate balance of hydrophobic and hydrophilic interactions. Due to their amphiphilic structure, surfactants feature further manifestations of hydrophobicity such as aggregation, liquid crystals, or microemulsions [2]. This special behavior makes conventional parameterization strategies difficult to apply. It favors the use of GC methods since the experimental data of surfactants required for this parametrization are contaminated by the spontaneous formation of aggregates, making them ill-defined. Moreover, GC methods allow to describe an entire surfactant class with a single parameter set, which conversely means that well-defined and independent data can be used to parametrize the individual groups. However, GC methods rely on the premise that the (effective) properties of a molecule can be determined from the contributions of the individual functional moieties of that compound. Thus, the individual domain-specific interactions must be accurately represented, which directly leads to the task of modeling the special interactions between hydrophobic groups (forming surfactant tails) and water, which was addressed above in detail.

Towards this goal, in this work we employed the hetero-segmented PC-SAFT developed by Haarmann et al. [24,31] for homologous series of polar and self-associating long-chain compounds. This work aims to further develop this approach and to completely disassemble the molecules into functional groups. We choose CH_2, CH_3, and CH_2OH groups for this purpose and will propose a method to explicitly account for the hydrophobic effect to improve the description of aqueous systems that contain hydrophobic moieties. The model will be applied to pure-component properties of n-alkanes and n-alcohols, binary mixtures thereof as well as to mixtures of these compounds with water.

2. Theory

2.1. Calculation of thermodynamic properties

In this work, all thermodynamic properties and phase equilibria were calculated using PC-SAFT, which is a model for the molar residual of the Helmholtz energy a^{res} as a function of molar density ρ, temperature T, and composition $\vec{x}$. Once this is known, any other thermodynamic property can be obtained applying textbook thermodynamics [32]. In the following we summarize this for the properties considered in this work.

The molar density ρ at given pressure p and temperature was calculated by solving the following implicit equation.

$$p = \rho RT\left(1+\rho\frac{\partial(a^{res}/RT)}{\partial\rho}\right) \tag{1}$$

In Eq. (1), R is the universal gas constant.

Vapor–liquid (VLE) and liquid–liquid (LLE) phase equilibria were calculated by applying the isofugacity criteria according to

$$(x_i\varphi_i)^1_{p,T,\vec{x}_1} = (x_i\varphi_i)^j_{p,T,x_j}\, i = 1,\ldots,N_C, j = 2,\ldots,N_P \tag{2}$$

Corresponding to this phase-equilibrium condition, the product of the mole fraction of component i with its fugacity coefficient φ_i must be the same in all N_P phases. The fugacity coefficient of component i as a function of pressure and temperature is obtained by differentiation of the residual Helmholtz energy with respect to its mole fraction x_i according to the following equation

$$\ln(\varphi_i) = \frac{a^{res}}{RT} + \frac{\partial(a^{res}/RT)}{\partial x_i} - \sum_{j=1}^{N_C-1} x_j\frac{\partial(a^{res}/RT)}{\partial x_j} + Z - 1 - \ln(Z) \tag{3}$$

In this equation, $Z = p/\rho RT$ stands for the compressibility factor. The activity coefficient γ_i is related to the fugacity coefficient through the following expression

$$\gamma_i = \frac{\varphi_i}{\varphi_{0i}} \tag{4}$$

Thus, the activity coefficient was obtained by relating the fugacity coefficient of a component in the mixture φ_i to its pure-component fugacity coefficient φ_{0i} at the same temperature and pressure.

Solid–liquid phase equilibria (SLE) were calculated using the following equation.

$$\ln(x_i) + \ln(\gamma_i) = -\frac{\Delta h_i^{SL}}{RT}\cdot\left(1-\frac{T}{T_i^{SL}}\right) - \frac{\Delta c_{p,i}^{SL}}{R}\cdot\left[\ln\left(\frac{T_i^{SL}}{T}\right) - \frac{T_i^{SL}}{T} + 1\right] \tag{5}$$

Here, Δh_i^{SL} is the melting enthalpy, T_i^{SL} is the melting temperature, and $\Delta c_{p,i}^{SL}$ is the change in isobaric heat capacity upon melting. Solving this equation to the mole fraction x_i gives the solubility of this component.

The excess enthalpy h^E was calculated through the following expression

$$\frac{h^E}{RT} = \frac{h^{res}}{RT} - \sum_{j=1}^{N_C} x_j\frac{h_{0j}^{res}}{RT} \tag{6}$$

In this relation, h^{res} and h_{0j}^{res} are the residual enthalpy of the mixture and of the pure components j, respectively. The residual enthalpy was obtained by differentiation of the residual Helmholtz energy with respect to the temperature according to

$$\frac{h^{res}}{RT} = -T\frac{\partial(a^{res}/RT)}{\partial T} + Z - 1 \tag{7}$$

The residual heat capacity c_p^{res} is obtained through a further differentiation with respect to the temperature according to

$$\frac{c_p}{R} = \frac{c_p^{iG}}{R} + \frac{\partial(h^{res}/RT)}{\partial T} \tag{8}$$

The isobaric heat capacity in the ideal gas state c_p^{iG} was computed via correlation functions, which were readily available for all substances considered in this work.

Another property considered in this work is the octanol/water partition coefficient K_{OW}. Assuming the two liquid phases are in equilibrium, this quantity was calculated as follows

$$K_{OW} = \frac{\gamma_i^{\infty,aq}}{\gamma_i^{\infty,org}}\frac{\rho^{org}}{\rho^{aq}} \tag{9}$$

$\gamma_i^{\infty,aq}/\gamma_i^{\infty,org}$ is the ratio of the infinite-dilution activity coefficients of the solute in the water-rich phase and in the n-octanol-rich phase, respectively. The compositions of the two phases were obtained through solving Eq. (2). ρ^{org}/ρ^{aq} is the ratio of the molar densities of the two phases.

The Henry's law constant H_{ij} quantifies the equilibrium concentration of a solute i dissolved in a solvent j at a given temperature and pressure. This quantity was obtained as follows

$$H_{ij} = \varphi_i^{\infty}\left(T, p_j^{LV}\right)\, p_j^{LV} \tag{10}$$

In this equation, $\varphi_i^{\infty}(T, p_j^{LV})$ is the infinite-dilution fugacity coefficient of the solute in the liquid at temperature T and vapor pressure of the solvent p_j^{LV}.

2.2. Hetero-segmented PC-SAFT

PC-SAFT represents a molecule as a chain of hard spheres tangentially bounded with each other [13]. The model describes the residual Helmholtz energy a^{res} to consist of independent contributions. The ones

considered in this work are

$$a^{res} = a^{hc} + a^{disp} + a^{assoc} \tag{11}$$

The term a^{hc} represents the hard-chain reference system. The second term a^{disp} accounts for the dispersive interactions of van der Waals type. The third term a^{assoc} accounts for quasi-chemical forces, which are typically of hydrogen-bonding type [33]. Several further contributions can be included to account for special interactions, for instance long-range Coulombic forces. Further information and detailed insight into the single contributions for the homo-segmented approach are readily available in the literature [13,14,34].

The hetero-segmented incarnation of PC-SAFT used in this work is based on the procedure proposed by Gross et al. [35] and advanced by Haarmann et al. [24,31]. The detailed equations for the hetero-segmented approach can be found in the original publications. Accordingly, the molecule is subdivided into various groups, each constituted by a set of identical but group-specific segments. A component consisting of only one group corresponds to the homo-segmented description.

Generally, modeling a system in this GC approach requires group parameters and information about group multiplicity and connectivity. Each group is described by six parameters: the number of segments (m_i), the segment diameter (σ_i), the dispersion-energy parameter (u_i /k_B), the number of association sites (N_i^{Assoc}) for each association type, the association-energy parameter ($\varepsilon^{A_iB_i}/k_B$) and the association volume ($\kappa^{A_iB_i}$). Only two different types of association sites are considered, abbreviated with A and B.

This approach employs combining rules even for pure-component calculations to compute the unlike-group potential parameters based on the pure-group potential parameters

The dispersion parameters (u_{ij} and σ_{ij}) for a pair of unlike groups are obtained by the modified Berthelot–Lorentz combining rules

$$u_{ij} = \sqrt{u_i u_j}\,\left(1 - k_{ij}\right) \tag{12}$$

$$\sigma_{ij} = \frac{\sigma_i + \sigma_j}{2}\,\left(1 - l_{ij}\right) \tag{13}$$

The parameters k_{ij} and l_{ij} are called binary interaction parameters (BIPs). Due to the way they enter the SAFT equations, the two BIPs are strongly correlated. Therefore, the l_{ij} can be equated to zero without loss of generality [36]. Although it is desirable to neglect the k_{ij} to maintain a predictive character of the modeling, it was shown that for mixtures of even simple polar molecules the k_{ij} is non-zero and even temperature dependent [37]. Eventually, k_{ij} also corrects any other shortcomings than only the one of a^{disp}, e.g. model imperfections due to imposing the one-fluid theory or due to the method to extend PC-SAFT to hetero-segmented chains. Throughout this work, the following equation was used to correlate the k_{ij} as a function of temperature

$$k_{ij} = k_{ij,0} + \frac{k_{ij,1}}{T} \tag{14}$$

The parameters $k_{ij,0}$ and $k_{ij,1}$ were adapted to experimental data. The inverse temperature dependence was motivated by Haslam's [37] analytical results and accounts for any polar interactions between unlike molecules/groups.

Cross-association between unlike groups is governed by the cross-association strength $\Delta^{A_iB_j}$ according to

$$\Delta^{A_iB_j} = g_{ij}^{HS}\ \sigma_{ij}^3\ \kappa^{A_iB_j}\left[\exp\left(\frac{\varepsilon^{A_iB_j}}{k_BT}\right) - 1\right] \tag{15}$$

This relationship approximates the number of molecules within the maximum distance at which association can occur by the value of the hard-sphere radial distribution function at contact g_{ij}^{HS} times the association volume $\kappa^{A_iB_j}$ [38]. The association energy $\varepsilon^{A_iB_j}$ describes the temperature dependence of the association strength. The association parameters of unlike groups $\kappa^{A_iB_j}$ and $\varepsilon^{A_iB_j}$ are calculated via the combining rules of Wolbach and Sandler [39].

$$\varepsilon^{A_iB_j} = \frac{\varepsilon^{A_iB_i} + \varepsilon^{A_jB_j}}{2}\left(1 - k_{ij}^{HB}\right) \tag{16}$$

$$\kappa^{A_iB_j} = \left(\sqrt{\kappa^{A_iB_i}\ \kappa^{A_jB_j}} + l_{ij}^{HB}\right)\left(\frac{\sqrt{\sigma_i\sigma_j}}{\sigma_{ij}}\right)^3 \tag{17}$$

The BIPs k_{ij}^{HB} and l_{ij}^{HB} serve the same purpose as the k_{ij} and are usually adapted to experimental data. Commonly, these BIPs are set to zero and any deviations so introduced are corrected by the k_{ij} (Eq. (14)). On the other hand, the k_{ij}^{HB} and l_{ij}^{HB} BIPs provide access to generally account for solvation phenomena. This was for example used by Kleiner and Sadowski [30] to model the fact that the presence of a self-associating molecule induces cross-association with another non-associating molecule, which is called induced association.

It was shown in various studies, that the incorporation of the solvation effects via the induced association increased the accuracy and predictive power of PC-SAFT significantly [30,40]. As mentioned in the introduction, Tan et al. [25] made use of this approach to account for polar interactions between small hydrocarbons and water with promising results.

3. Modeling hydrophobic interactions

3.1. Modeling strategy

Currently, for an n-alkane/water system at a constant temperature, only the k_{ij} can be adjusted by tuning the dispersive interactions between these molecules. As a result, either the aqueous phase or the organic phase is correlated with significant deviations in the conjugated phase. This indicates that the complex interactions between water and hydrophobic molecules cannot be adequately represented by dispersive interactions alone. This observation motivated the development of a novel approach to explicitly account for other than dispersive interactions. The method introduced in this work is similar to the work of Tan et al. [25] with the difference that we aimed for a separate modeling of direct contributions due to pair-wise van der Waals interactions on the one side and indirect contributions due to the hydrophobic effect on the other side.

We assume that all direct contributions (dispersive as well as polar interactions) can be captured by the dispersion term in combination with the k_{ij} according to Eq. (14) [37]. Our approach to consider the hydrophobic effect is based on the desire to retain the current PC-SAFT framework. As stated in the introduction, the energetic state of a solution subject to the hydrophobic effect is caused by a complex interplay of enthalpic and entropic driving forces, presumably based on the influence of the hydrophobic components on the water structure [3,4,41]. Since this cannot be explained by an effective pair potential, there is little possibility of modeling this directly with PC-SAFT.

However, the hydrophobic effect induces apparent attractive forces between hydrophobic molecules: so-called hydrophobic interactions [4,7,42,43]. As these hydrophobic interactions are known to cause so-called hydrophobic association [42,43], the use of the association contribution a^{assoc} promises access to account for these solvent-mediated interactions. This Helmholtz-energy contribution processes the monomer mole fraction as the key property, i.e. the fraction of molecules being singly dispersed. Any value less than one results in a negative contribution to the residual Helmholtz energy. In the case of hydrophobic molecules, this expresses the energetic advantage of not being in contact with water. Therefore, the task is to model a monomer mole fraction of the hydrophobic component. To ensure a well-defined generalization to both pure hydrophobic component systems and multicomponent mixtures, this model must satisfy an important constraint: if no water is present in the mixture, the monomer fraction of

the hydrophobic component must be equal to one. A suitable method that fulfills this restriction is to impose cross-association between water and hydrophobic molecules. To enable cross-association, the cross-association strength $\Delta^{A_iB_j}$ between water and the hydrophobic component must be modeled.

For model development and validation of the new approach, we performed preliminary studies in the framework of homo-segmented PC-SAFT, in which the LLEs of binary n-alkane/water mixtures were investigated. At different temperatures, we adapted the dispersive BIP k_{ij} as well as the normalized association strength $\Delta^{A_iB_j}/g_{ij}^{HS}\,\sigma_{ij}^3$ (instead of either k_{ij}^{HB} or l_{ij}^{HB}) between water and the n-alkane to the compositions of the two equilibrium phases. That procedure revealed that k_{ij} was almost perfectly linear with respect to the inverse temperature whereas $\Delta^{A_iB_j}/g_{ij}^{HS}\,\sigma_{ij}^3$ was zero at low temperatures and linearly increased after passing a temperature of 270 K. This resulted in a progressively higher degree of hydrophobic association as the temperature surpasses 270 K.

Whereas the temperature dependence of the k_{ij} is plausible from a theoretical point of view (Eq. (14)), the increase of the association strength with temperature contrasts the physical concept in which the degree of association decreases with temperature (Eq. (15)). This discrepancy is explained by applying a physics-based theory to a topic for which it was not developed for. On the other hand, the literature reports various theoretical works that confirmed that rising temperatures favor hydrophobic interactions [42–45]. Lüdemann et al. [42,43] studied the behavior of two methane molecules dispersed in water through atomistic simulations at different temperatures. They demonstrated the increase of hydrophobic association with temperature and that this behavior is initialized in a narrow temperature range of around 300 K. Furthermore, their results suggest that hydrophobic association vanishes for low temperatures. Although our approach to model hydrophobic interactions is pragmatic, the necessary temperature dependence of the cross-association strength aligns well with their results.

Supported by the findings above, we concluded that our approach succeeds in depicting the hydrophobic interactions separately to direct contributions due to pair-wise van der Waals interactions. However, we modified the expression to calculate the cross-association strength to avoid temperature-dependent associative BIPs (l_{ij}^{HB} or k_{ij}^{HB}). We propose Eq. (18) for the association strength $\Delta^{A_iB_j}$ between CH_X groups and water, which is an empirical and simple relations but accurately describes the temperature dependence of the association strength.

$$\Delta^{A_iB_j} = g_{ij}^{HS}\,\sigma_{ij}^3\,l_{ij}^{HB}\,\log[1+\exp(T/K-270)] \tag{18}$$

This equation computes the cross-association strength with only one BIP l_{ij}^{HB}, named equal to the one used in the conventional framework. The transition temperature was fixed at 270 K to counteract overfitting. The logarithmic factor is equal to zero for temperatures below 270 K and is exactly linear with respect to temperature when above 270 K.

This methodology is readily applied also in the hetero-segmented PC-SAFT by enabling cross-association between a hydrophobic group and water according to Eq. (18). For any other functional groups used within the hetero-segmented approach, the cross-association strength is computed conventionally via Eq. (15).

3.2. Parameter estimation

This work first considers the parameterization of CH_2 and CH_3 groups as these are the most prominent functional groups in the context of hydrophobic interactions. We added CH_2OH to the portfolio of functional groups to also describe n-alcohols. From these groups, alkanes and alcohols of any length can be constructed. This allowed us to evaluate the model performance for modeling the families of n-alkanes and n-alcohols using the same parameters. To describe aqueous mixtures, also pure-component parameters of water are required. The parameters used in this work were taken from the literature [46]. This water model assumes a 4C association scheme, which was found to be superior to the 2B scheme for the description of the mutual solubility in aqueous mixtures of n-alkanes [47]. This was confirmed by Haarmann et al. [12], who achieved good results in modeling the mutual solubilities in n-alkane/water mixtures using this parameter set for water.

Thus, group parameters as well as BIPs have been required. Between CH_2, CH_3, and CH_2OH groups only the dispersive BIP k_{ij} was used. The interactions between water and the functional groups were tuned via the BIPs k_{ij}, l_{ij}^{HB}, and k_{ij}^{HB}. The CH_2 group and the CH_3 group were assigned a single association site of donor type to enable the cross-association with water (Section 3.1). The CH_2OH group is modeled with the 2B association scheme.

The parameterization took place in two steps. First, we adapted the parameters for the CH_2, CH_3, and CH_2OH groups and BIPs between these groups. Subsequently, we adapted the BIPs between these groups and water. Even if the primary goal was to describe aqueous solutions, this approach served to give the groups as much physics as possible. Simultaneous adaptation of group parameters to the phase behavior with water would result in the fact that any deficiencies are compensated by the pure-group parameters, which would be at the expense of their physical significance and reliability for extrapolation.

Each parameterization step led to a multi-criteria optimization. The target function F was defined by summing up all objectives with equal weight with the restriction that each objective must be fulfilled to a certain degree. This served as an instrument to avoid overfitting. Each individual objective f was defined as follows

$$f = \frac{1}{N_D}\sum_{i=1}^{N_D}\left|\frac{y_i^{exp}-y_i^{calc}}{y_i^{exp}}\right| \tag{19}$$

This expression equals the definition of the Average Absolute Relative Deviation (*AARD*). In this equation, N_D quantifies the number of experimental data points for each objective (for example vapor pressure) and y_j defines the thermodynamic property, either the experimental or the calculated value. The target function F was minimized using a combination of a global evolutionary-based minimizer and a local derivative-free minimizer to obtain the global minimum.

Whenever possible, we used data correlations instead of experimental raw data for parameter fitting. This is advantageous in several ways. First, when properly parametrized, these correlations provide consistent data not only as a function of temperature but also as a function of the carbon length. Second, using smoothed data for fitting makes incorporating uncertainties into objective function unnecessary.

Different regularization strategies were applied. These strategies refer to a family of methods to adjust the model capacity to the current data set, i.e. how many parameters are *really* necessary to explain the data, to eventually avoid overfitting and improve the generalization behavior. [48]

4. Results and discussion

4.1. Estimation of group parameters

The parameters for the CH_2, CH_3, and CH_2OH groups and the BIPs between these groups were obtained by adjusting them simultaneously to data on vapor pressures and saturated-liquid densities of the homologous series of n-alkanes and n-alcohols. This way, the CH_X groups were parameterized without the information whether or not this group is part of an n-alkane or of an n-alcohol. The experimental data were generated using the correlations published by Yaws Handbook of Thermodynamic Properties [49]. For regression, we considered n-alkanes/n-alcohols with a number of carbon atoms from C_4 to C_{14} in the reduced temperature range from 0.5 to 0.9. Short-chain molecules were excluded because these representatives fundamentally differ in their electrostatic characteristics from the other homologues due to proximity effects [16, 50–52]. Restriction to molecules of up to 14 carbon atoms served a dual

purpose. First, many accurate data are available for these molecules and second, as we are interested in extrapolation, the comparison with data on long-chain molecules gives a good estimate for the generalization behavior. The reduced temperature range from 0.5 to 0.9 covers a broad temperature range from 212 K (reduced temperature of 0.5 for n-butane) up to 670 K (reduced temperature of 0.9 for n-tetradecanol).

Due to the GC nature of the model, not only n-alkanes or n-alcohols of any length but also n-alkane/n-alcohol mixtures can be modeled without requiring additional parameters. We made use of this fact and added data on isobaric vapor–liquid-equilibria (VLE) of the n-heptane/n-pentanol mixture to the data set for regression [53]. This provided independent information and counteracted overfitting. Furthermore, the data on the isobaric VLE give valuable information about the temperature dependence of activity coefficients. The obtained parameters for the CH_2, CH_3, and CH_2OH groups and the BIPs k_{ij} are listed in Tables 1 and 2. These parameters belong to a distinct global optimum and no challenge in terms of parameter degeneracy was observed. The regularization strategies (Section 3.2) resulted in temperature-independent BIPs.

Using this parameter set, the model approach fitted the vapor pressures and the saturated-liquid densities of both n-alkanes and n-alcohols as well as the VLE of the n-heptane/n-pentanol mixture with average residuals below 3 %. This is specified by Fig. 1, illustrating the *AARD* of the n-alkanes (a) and n-alcohols (b) as functions of the reduced temperature. *AARDs* were obtained by averaging over all systems at a specific reduced temperature. The vapor pressures of the n-alkane series were described slightly better than the ones of the n-alcohols, which may be attributed to the model assumption that the degree of association is unaffected by the component length, i.e. the model does not account for any steric hindrance. No dependence was found for the *AARD* as a function of chain length. Thus, the model described both homologous series evenly well. Fig. 1a and b also show the *AARDs* when applying the homo-segmented approach to the same experimental data using parameters from literature ([13] for n-alkanes, [14,55] for n-alcohols). Similar results as for the hetero-segmented approach were found but with individual parameters for each compound.

Fig. 1c shows the VLE of the binary n-heptane/n-pentanol mixture along with the computations of the hetero-segmented model and homo-segmented model. The hetero-segmented model accurately correlates the phase behavior with special regard to the azeotropic point. In comparison to the homo-segmented approach, the hetero-segmented model describes the VLE slightly better, although the model was not parameterized to this data alone. The homo-segmented approach was fitted using the constant BIP $k_{ij,0}$ which is provided in the Appendix.

For validation, the parameters obtained in this work were compared to existing parameters for the homo-segmented approach [13,14,55]. This was done for the parameter combinations m, $m\sigma^3$, and $mu\ /k_B$, which are known to show well-defined trends for homologous series thus combining the parameters physically [40]. In the hetero-segmented approach, these parameter combinations were obtained by summing over all groups of the component weighted by their multiplicity. Fig. 2a shows this comparison for n-alkanes disclosing striking accordance. Particularly agreement exists for the combination $m\sigma^3$, related to the hard-core molecular volume often used as a molecular descriptor in computational chemistry [56–58]. The agreement in molecular volume predictions across these two different incarnations of PC-SAFT suggests that the fundamental principles underlying both approaches capture the essential features of the fluid behavior in a consistent manner. Additionally, the parameters for the CH_2 group resemble the parameters for polyethylene (PE) (compare Table 1) manifesting their physical relation as a model result.

Table 2
Group interaction parameters for hetero-segmented PC-SAFT determined in this work.

Group 1	Group 2	$k_{ij,0}/-$
CH_2	CH_3	−0.08271
CH_2	CH_2OH	0.02018
CH_3	CH_2OH	0.1198

Analogously, Fig. 2b illustrates the same comparison for the n-alcohols, again with reasonable agreement. Again, the combination $m\sigma^3$ is in close relation to the trend defined by the parameter of the homo-segmented approach. Likewise, the association parameters of the CH_2OH group were found to be within the range of the representatives of homo-segmented PC-SAFT (not shown). Additionally, the association energy of 2676 K agrees with the experimental range of 2500–3000 K [59].

The model performance was further evaluated comparing predictions with data not used for regression. For this purpose, we chose the isobaric heat capacity, as this property is particularly sensitive to the energy parameters (dispersion energy, association energy) and is often used as a benchmark to test the predictive ability of the thermodynamic model [60]. The ideal heat capacities were computed according to correlations available in the literature [49]. Fig. 3a (n-alkanes) and Fig. 3b (n-alcohols) compare the prediction with experimental data.

The n-alkanes are described very precisely up to high temperatures near the critical temperature. The n-alcohols are also described almost quantitatively at lower temperatures with minor deviations at higher temperatures. Overall, the quality of the prediction is remarkable and suggests that the parameterization correctly describes the balance of intermolecular energies between different functional groups.

The extrapolation capabilities of the group parameters were confirmed by comparing the predicted and experimental vapor pressures of n-eicosane (C_{20}) and n-eicosanol ($C_{20}OH$) which are in extraordinary agreement over a wide temperature range (Fig. 4). These results undoubtedly demonstrate the model's potential for consistent extrapolation, having in mind that the fitting took place considering n-alkanes and n-alcohols only up to fourteen carbon atoms.

4.2. n-alcohol/n-alkane mixtures

The model allows us to model the phase behavior of any n-alkane/n-alcohol mixture using the parameters listed in Tables 1 and 2, which was used for validation purposes. Except for the VLE of the n-pentanol/n-heptane mixture, these computations were purely predictive, as no other data were used for parameter estimation.

Fig. 5 illustrates the *AARD* values for n-alkane/n-alcohol VLEs for both the hetero-segmented approach and the homo-segmented approach. The experimental data for the computation of the *AARD* were taken from the literature [53,67–77]. Whereas the calculations of the hetero-segmented approach were purely predictive, a constant BIP

Table 1
Group parameters for hetero-segmented PC-SAFT determined in this work. The parameter sets for polyethylene (PE) and water were taken from the literature.

Group	$mM_i^{-1}/molg^{-1}$	$\sigma_i/\mathring{A}$	$u_i k_B^{-1}/K$	$\kappa^{A_iB_i}/-$	$\varepsilon^{A_iB_i}\ k_B^{-1}/K$	N_i^{Assoc}	Ref.
Water	0.1414	2.105	138.6	0.2912	1718	2:2	[46]
CH_2	0.02679	3.994	259.3	0	0	1:0	this work
PE	0.02630	4.022	252.0	0	0	0:0	[54]
CH_3	0.05841	3.437	177.5	0	0	1:0	this work
CH_2OH	0.02292	4.066	401.0	$5.833{\cdot}10^{-4}$	2676	1:1	this work

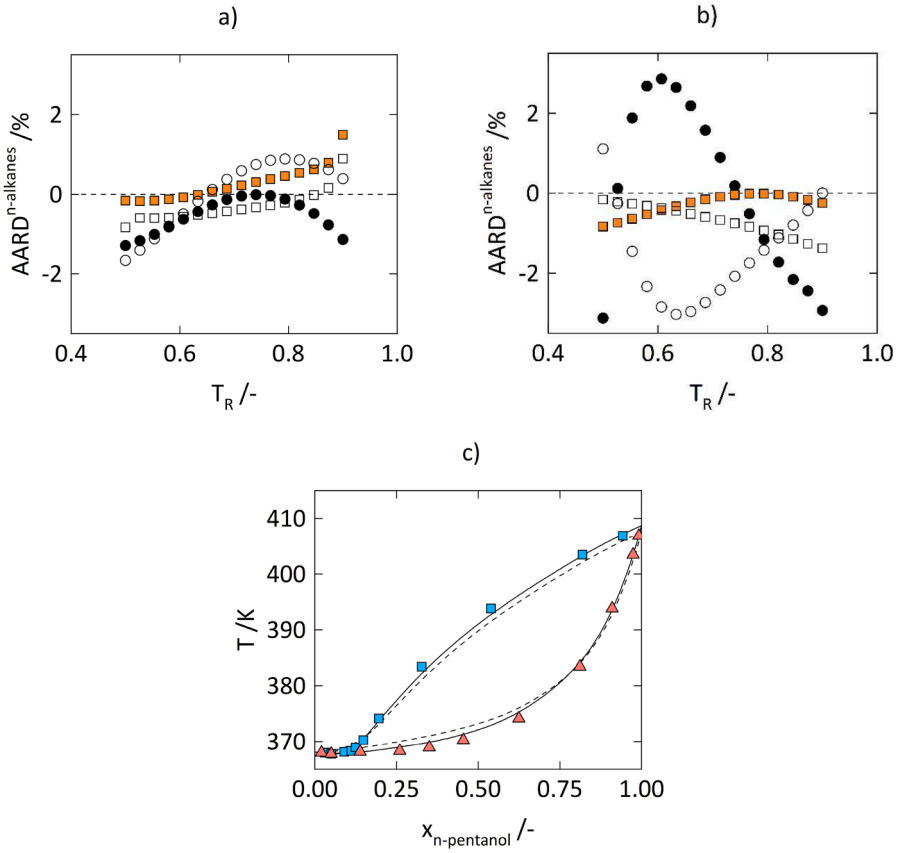

Fig. 1. Average absolute relative deviations for the saturated-liquid density (squares) and vapor pressure (circles) as functions of the reduced temperature a) n-alkanes, b) n-alcohols. Filled symbols correspond to the hetero-segmented approach, empty symbols to the homo-segmental approach. c) VLE of the n-pentanol/n-heptane system at 0.91 bar. Squares (dew points) and triangles (boiling points) are experimental values [53]. Solid lines are from the hetero-segmented approach, dashed lines are from the homo-segmented approach.

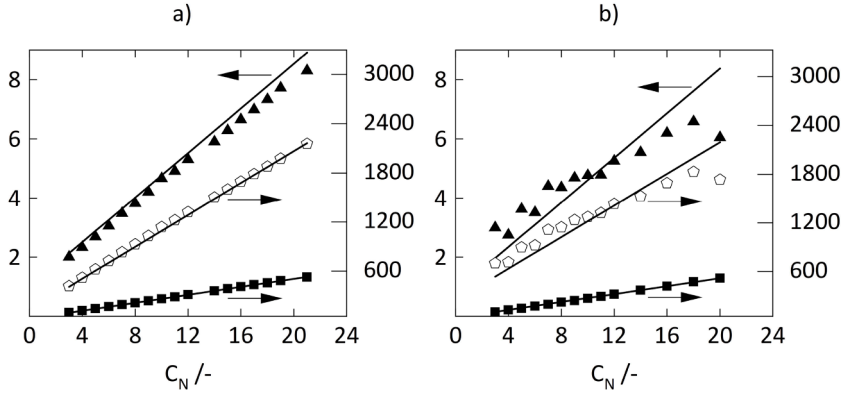

Fig. 2. Segment number $m/-$ (triangles), molecular volume $m\sigma^3/\text{Å}^3$ (squares) and molecular dispersion energy muk_B^{-1}/K (empty pentagons) as functions of the carbon number for n-alkanes (a) and n-alcohols (b). Solid lines correspond to the hetero-segmented parameters. Symbols denote parameters of the homo-segmented approach taken from the literature [13,14,55].

$k_{ij,0}$ was fitted for the homo-segmented model to each VLE separately (provided in the Appendix). This grants the homo-segmented approach greater flexibility to regress experimental data (even inaccurate ones) compared to the hetero-segmented approach. Taking this into account, the results of the new parameterization are very impressive. In direct comparison, the two methods perform almost equally well.

Equipped with BIPs adapted to VLE data, the two approaches were then used to predict the SLE in the same systems. The melting properties (used within Eq. (5)) and experimental data were taken from Literature [75,78–80]. Fig. 6 depicts the *AARD* values for these predictions. Obviously, the hetero-segmented approach outperforms the homo-segmented approach without exception, quantified by an average *AARD* less than half the value of the homo-segmented approach. As examples, Fig. 7 shows the phase diagrams (VLE and SLE) of the n-butanol/n-octane mixture (a) and n-octanol/n-decane mixture (b).

These results demonstrate the extrapolation capabilities of the hetero-segmented approach to binary mixtures over a broad temperature range, consistently predicting thermodynamic data not used for the

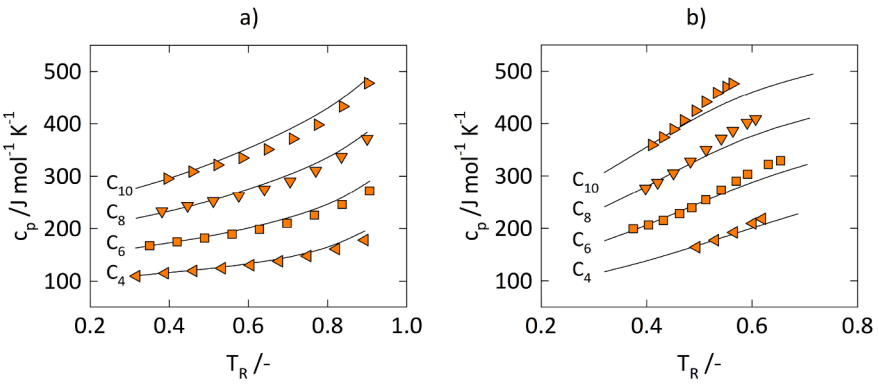

Fig. 3. Saturated-liquid isobaric heat capacities as functions of reduced temperature for n-alkanes (a) and n-alcohols (b). Experimental data [49,61,62] are depicted as circles (10 carbon atoms), diamonds (8 carbon atoms), squares (6 carbon atoms), and triangles (4 carbon atoms). Solid lines are predictions from the hetero-segmented approach.

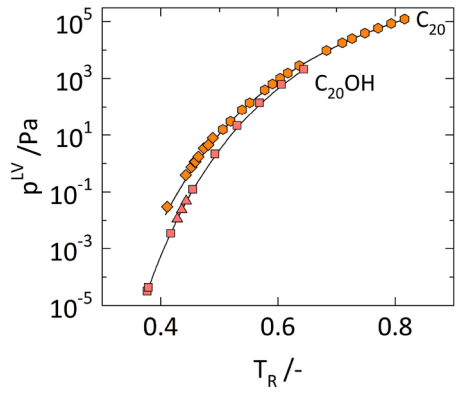

Fig. 4. Pure-component vapor pressures as functions of temperature for n-eicosane (C_{20}) and n-eicosanol ($C_{20}OH$). Experimental data are depicted as triangles [63], squares [64], diamonds [65] and hexagons [66]. Solid lines are predictions from the hetero-segmented approach.

parameterization. This trend continues when predicting the excess enthalpy, illustrated by Fig. 8 for the n-butanol/n-pentane mixture and n-butanol/n-octane mixture. The new parameterization correctly predicts positive values as well as the asymmetry of the excess enthalpy as a function of the composition. In comparison, the new parameterization again outperforms the homo-segmented approach.

The above findings demonstrate the performance of the hetero-segmented approach to describe the homologous series of *n*- n-alkanes and n-alcohols accurately in the same quality as when applying the homo-segmented approach. The new parameterization also performs equally well on unseen data and extrapolates accurately.

4.3. Liquid–liquid equilibria of n-alkanes and n-alcohols with water

The main focus of this work was modeling the aqueous phase behavior subject to the hydrophobic effect. This is directly related to the mutual solubilities in binary mixtures of hydrophobic components and water. For that purpose, the BIPs k_{ij}, l_{ij}^{HB} and k_{ij}^{HB} between the CH_2, CH_3, and CH_2OH groups on the one hand and water on the other hand were adjusted simultaneously to data o LLE of water/n-alkane and water/n-alcohol systems (from C_5 to C_8) in the temperature range from 270 K

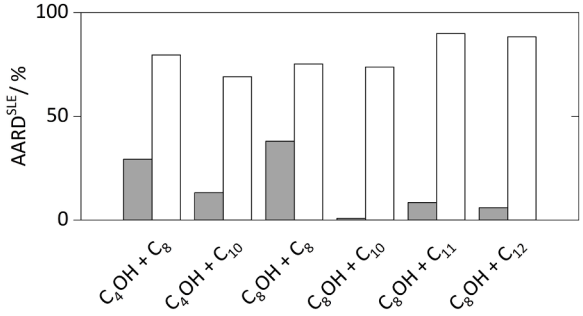

Fig. 6. Average absolute relative deviations for SLEs of n-alkane/n-alcohol mixtures. Grey bars are the results using the hetero-segmented approach, white bars are from the homo-segmented approach. The n-alkanes are abbreviated as C_N. The n-alcohols are abbreviated as C_NOH.

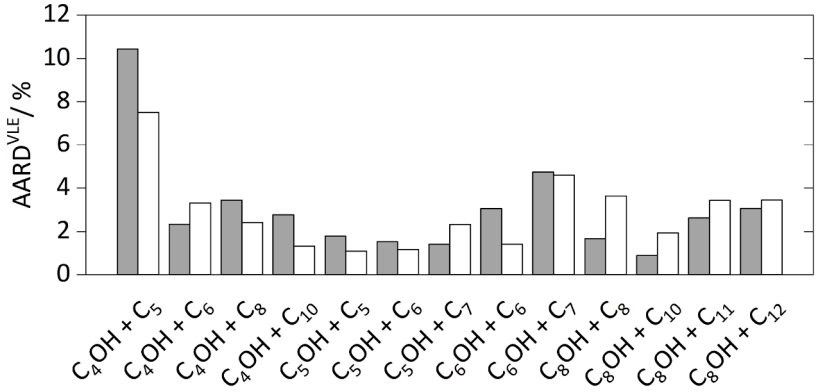

Fig. 5. Average absolute relative deviations for VLEs of n-alkane/n-alcohol mixtures. Grey bars are the results using the hetero-segmented approach, white bars are the ones from the homo-segmented approach. n-alkanes are abbreviated as C_N. n-alcohols are abbreviated as C_NOH.

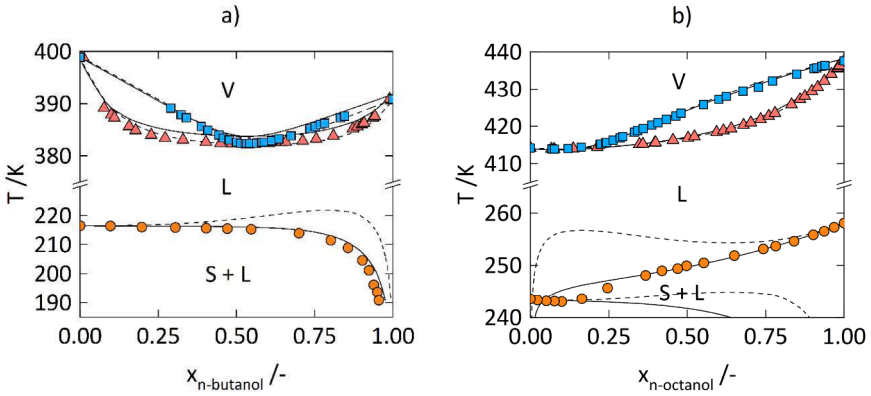

Fig. 7. Phase diagrams (SLE and VLE) of (a) n-butanol/n-octane mixture at atmospheric pressure and (b) n-octanol/n-decane mixture at 0.4 bar. V stands for vapor, L for liquid, and $S + L$ for the two-phase region in which solid is in equilibrium with saturated liquid. Squares and triangles are dew points and boiling points, respectively [69,76]. Circles are solubilities [78,79]. Solid lines are the predictive results from the hetero-segmented approach. Dashed lines were obtained using the homo-segmented approach with BIPs fitted to VLE data.

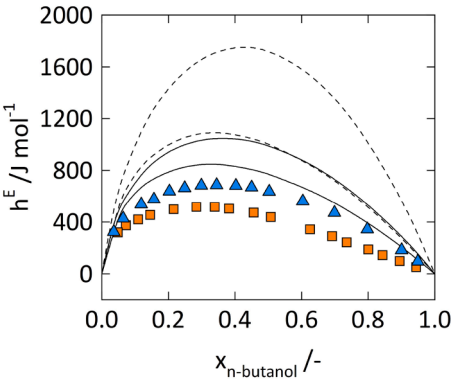

Fig. 8. Molar excess enthalpies at 298.15 K of the n-butanol/n-pentane mixture and n-butanol/n-octane mixture. Experimental data are shown as squares [81] (n-butanol/n-pentane) and triangles [82] (n-butanol/n-octane). Solid lines are the predictive results using the hetero-segmented approach. Dashed lines were obtained using the homo-segmented approach.

to 360 K. We adjusted these parameters to the compositions of the two phases and to all binary mixtures simultaneously. The systems used for regression were selected with regard to the reliability of experimental data. While fitting, we fixed the pressure for the calculations equal to atmospheric pressure. The data used for regression were generated using correlation functions proposed by Mączyński et al. [83], Góral et al. [84], and Tsonopoulos [5]. The parameters of the correlations were partly readjusted to our temperature range of 270 K to 360 K, using newly published data [41,85,86] and with special regard to a consistent chain-length dependence. The correlation functions and parameters are presented in the Appendix.

The BIPs for the CH_2, CH_3, and CH_2OH groups with water are listed in Table 3. Caused by the regularization strategies (Section 3.2), the dispersive BIPs $k_{ij,0}$ as well as the BIPs for the hydrophobic interactions (l_{ij}^{HB}) are the same for CH_2 and CH_3 groups. Regarding the dispersive BIPs dictating the temperature behavior ($k_{ij,1}$) for the two CH_X groups, they are both negative so that the attractive interactions between the CH_X groups and water weaken with temperature.

Table 3
Interaction parameters for hetero-segmented PC-SAFT between the CH_2, CH_3, and CH_2OH groups with water determined in this work. $k_{ij,0}$ and $k_{ij,1}$ compute the dispersive BIP as a function of temperature (Eq. (14)). l_{ij}^{HB} and k_{ij}^{HB} determine the cross-association strength.

Group	$k_{ij,0}$ / –	$k_{ij,1}$ /K	l_{ij}^{HB} / –	k_{ij}^{HB} / –
CH_2	0.4315	−69.13	0.001493[a]	–
CH_3	0.4315	−101.17	0.001493[a]	–
CH_2OH	0.1333	0	0.01915[b]	0

a) Used within a modified expression for the association strength (Eq. (18)).
b) Used within the conventional framework (Eqs. (15), (16), and (17)).

According to Section 2.2, the $k_{ij,1}$ correlates polar interactions between the CH_X groups and water. It is known that polar interactions generally decrease with temperature due to the increase in thermal motion [40]. Furthermore, the BIPs $k_{ij,1}$ of CH_2 and CH_3 groups with water follow a 2/3 ratio. This aligns with the ratio of the hydrogen atoms in these groups, which are the origin of the induced polar interactions with water. This temperature dependence of the dispersive BIP is consistent with other works applying the SAFT formalism to aqueous systems containing hydrocarbons, which state that k_{ij} increases with temperature to a high positive value [12,17,25]. Beside these physical validations, it is worth noting that the parameters $k_{ij,1}$ and $k_{ij,2}$ lead to a well-defined high-temperature limit of the dispersive interaction parameters k_{ij} of the CH_X groups with water ($k_{ij,\ T\to\infty} = 0.4315$). With respect to low temperatures, the interaction parameters k_{ij} of the CH_X groups with water stay reasonable ($k_{ij} > -0.1$) down to temperatures of 200 K.

The BIP for the hydrophobic interactions (l_{ij}^{HB}) was found to be very small leading to a cross-association strength order of magnitude smaller than the self-association of water. The results were extremely sensitive to this parameter.

Concerning the BIPs for the CH_2OH group with water, only two of four BIPs were found to be necessary as a result of the regularization strategies (Section 3.2). The dispersive BIP k_{ij} is positive and constant. The cross-association between the CH_2OH group and water is corrected only via the BIP l_{ij}^{HB}.

Using these parameters, the experimental data on mutual solubilities were fitted in a temperature interval from 270 K up to 360 K with an *AARD* of less than 6 % on average. This is specified in Fig. 9. The *AARD* was computed according to Eq. (19), using the water mole fraction in the organic phase and the hydrocarbon mole fraction in the aqueous phase. These results prove the expressiveness and efficiency of the hetero-segmented approach, as only six parameters were necessary to correlate both the organic and the aqueous phases of eight binary systems simultaneously and almost quantitatively. Neglecting the hydrophobic interactions ($l_{ij}^{HB} = 0$) led to a significant increase of the *AARD* and doing so, no parameter set was found that fits the data with an average *AARD* of less than 10 %. Therefore, the proposed method remarkably improves the model to the cost of in total only one more parameter (per group, not per system).

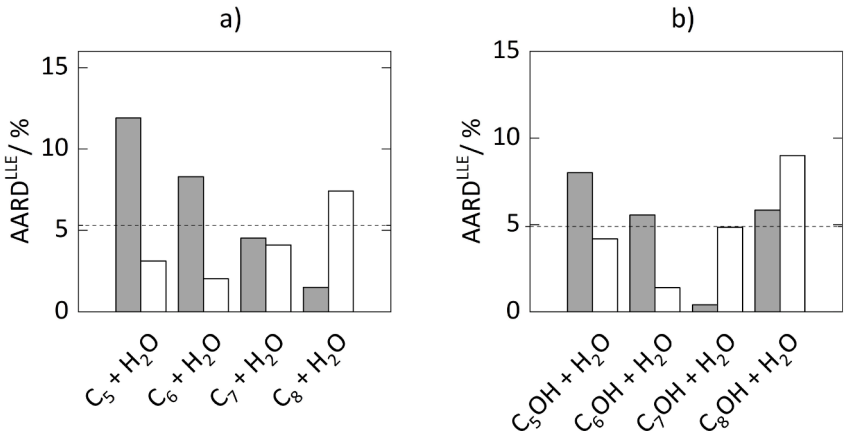

Fig. 9. Average absolute relative deviations for LLEs of the binary systems n-alkane/water (a) and n-alcohol/water (b) used for parameterization. Grey bars indicate the organic phase, white bars indicate the aqueous phase. The dashed lines give the average ***AARD***.

Fig. 10 shows the calculated phase boundaries using both homo-segmented and hetero-segmented approaches along with experimental data. Fig. 10a shows the results for n-alkane mixtures. Consistent with the low *AARD*, the calculated phases agree very well with the experimental data. The temperature behavior was exactly reproduced including the minimum in hydrocarbon solubility in the aqueous phase. Additionally, the model correctly extrapolates to higher temperatures, both in the aqueous and in the organic phase. The chain-length dependence was also captured precisely, which will be discussed further below. Fig. 10a also shows modeling results with the homo-segmented approach, for which the BIPs were taken from the literature [12] and provided in the Appendix. These parameters were adapted to the aqueous phase using a quadratic polynomial for the temperature dependence of the dispersive BIP (k_{ij}), separately for each mixture, which led to a total number of 12 parameters for the four binary systems, compared to four parameters in the new approach.

Despite the significant difference in the number of adjustable parameters, the two approaches perform equally well for the aqueous phase. However, the new approach can now for the first time also accurately represent the organic phase, whereas the homo-segmented approach exhibits an *AARD* for the organic phase of more than 15 %. Additionally, the inverse temperature dependence of the dispersive BIP (k_{ij}) ensures well-defined predictions even for high temperatures, whereas the quadratic correlations used in the homo-segmented approach should only be applied in the given temperature range.

Fig. 10b shows the results for the n-alcohol mixtures. Analogous to the n-alkanes, the solubility of n-alcohols in water is very well represented as a function of both chain length and temperature. As above, the model accurately extrapolates to higher temperatures. Significant deviations only occur for the n-butanol system. This system is the first one showing a miscibility gap with water. While larger alcohols also feature a miscibility gap with water, smaller alcohols are completely miscible over the entire temperature range. Despite the deviations observed in the system with n-butanol, the complete miscibility over the entire temperature range of both ethanol and propanol was also predicted with our model.

Regarding the solubility of water in the n-alcohols, visual deviations were present both along the temperature and carbon number axes. The results from the homo-segmented PC-SAFT approach are also shown, for which the BIPs ($k_{ij,0}$, $k_{ij,1}$ and l_{ij}^{HB}) were determined in this work using the same experimental data as before (provided in the Appendix). Using these parameters, the homo-segmented model approach describes the aqueous phase equally well for temperatures up to 360 K. For higher temperatures, beyond the region used for regression, the solubility is consistently underestimated. Remarkably, both approaches fit the organic phase almost equally well, even though the homo-segmented approach uses a multiple of parameters available compared to the hetero-segmented approach.

Fig. 11 compares the experimental and predicted chain-length dependencies at a constant temperature of 298.15 K, extrapolated to systems not used for parameterization. The n-alkane/water mixtures (Fig. 11a) are described with high precision. In accordance with the experimental data, the model predicts a rigorous exponential decrease in the solubility of the hydrophobic component in water. It is reported that

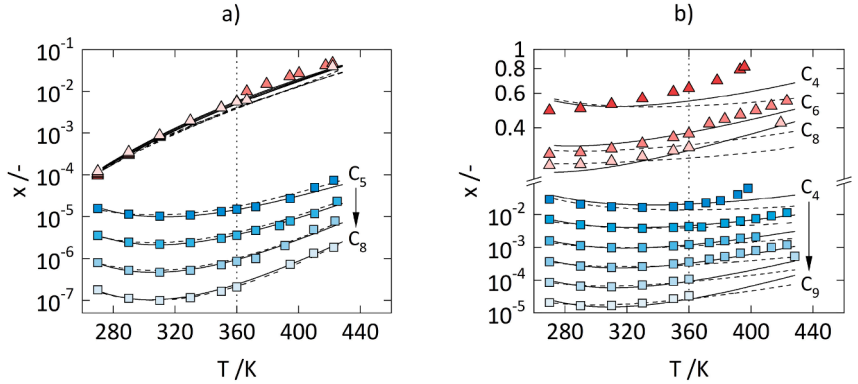

Fig. 10. Mutual solubilities in (a) n-alkanes/water mixtures and (b) n-alcohols/water mixtures at constant pressure as functions of temperature. Experimental data for the n-alkanes [83] and for the n-alcohols [84] are depicted as squares (solubility of the organic compound in water) and triangles (solubility of water in the organic phase). The symbol's transparency relates to the chain length. Solid lines are calculations using the hetero-segmented approach. Dashed lines are the correlations from the homo-segmented approach.

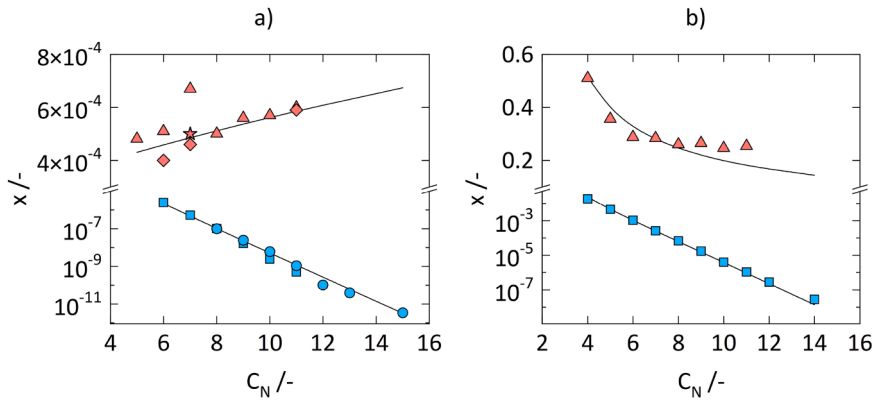

Fig. 11. Mutual solubilities in (a) n-alkanes/water mixtures and (b) n-alcohols/water mixtures at constant pressure and constant temperature of 298.15 K as functions of chain length. a) solubilities of the n-alkanes in water depicted as squares [83] and circles [87]. The solubility of water in the n-alkanes as triangles [83], diamonds [41], and stars [85]. b) solubilities of n-alcohols in water depicted as squares and the solubility of water in the organic phase as triangles [77]. Solid lines are calculations with the hetero-segmented approach.

this trend will maintain up to n-eicosane [2]. However, due to the exponential decrease in solubility, the uncertainties in the experimental data prevent any validation for n-alkanes longer than n-tetradecane. In contrast, the solubility of water in the organic phase is almost constant, which is also correctly predicted by the model. This can be explained by the self-association of water in the organic phase. Due to the high dilution, one can assume complete dissociation of any hydrogen bonds in the organic phase. Because the (partial molar) enthalpy accompanied with the dilution is almost constant, only a small dependence on the hydrocarbon chain length is expected [5], which is confirmed by the experimental data and captured by the model.

The n-alcohol/water mixtures (Fig. 11b) feature a similar behavior regarding the aqueous phase. As above, the predicted solubility of the hydrophobic component decreases exponentially in quantitative accordance with the experimental data. Similar to the n-alkanes, the same arguments hold for the attempt to validate the prediction with the experiment for higher n-alcohols. With respect to the organic phase, the water solubility decreases as a function of carbon length C_N, in contrast to the behavior of aqueous systems with n-alkanes. This is due to the fact that the water molecules are likely to undergo self- and cross-association in the organic phase with the hydroxyl group of the n-alcohol, resulting in a complex chain-length dependence and temperature dependence. The fact that the new model approach depicted this change in solubility dependence in very good accordance with the experimental data, once more highlights the physical foundation of the hetero-segmented model.

4.4. Predicting solvation properties in aqueous systems with n-alkanes or n-alcohols

In the following, our modeling approach will be validated via the prediction of new data sets. We will demonstrate that the new model approach can predict different types of phase equilibria over the entire range of composition including infinite-dilution regions.

First, we considered VLEs and VLLEs of binary mixtures composed of water and an n-alkane or an n-alcohol. Fig. 12 shows the phase diagrams for the water/n-octane mixture (a) and water/n-hexanol mixture (b) at atmospheric pressure.

Accordingly, the predictions are very good for the two systems. The model correctly predicts the boiling temperature and vapor composition, although these temperatures are beyond the consideration range during parameter fitting. We found equally good results for other VLEs of aqueous mixtures containing n-alkanes or n-alcohols (not shown). This proves the transferability of the parameters over a wide range of conditions.

Another quantity of interest is the activity coefficient at infinite dilution in water $\gamma_i^{\infty,aq}$, often used as a measure for hydrophobicity [8]. Fig. 13 compares the model predictions with experimental data for the n-alkanes and n-alcohols in water at a temperature of 298.15 K.

Depicted are experimental data with an uncertainty of less than one (in the logarithmic value) [90]. As to be seen, the predictions of $ln\ \gamma_i^{\infty,aq}$ are in quantitative agreement with the experimental data with no need for further improvements. The model predicts a strictly linear dependence of $\ln\gamma_i^{\infty,aq}$ with respect to the carbon number C_N for both n-alkanes

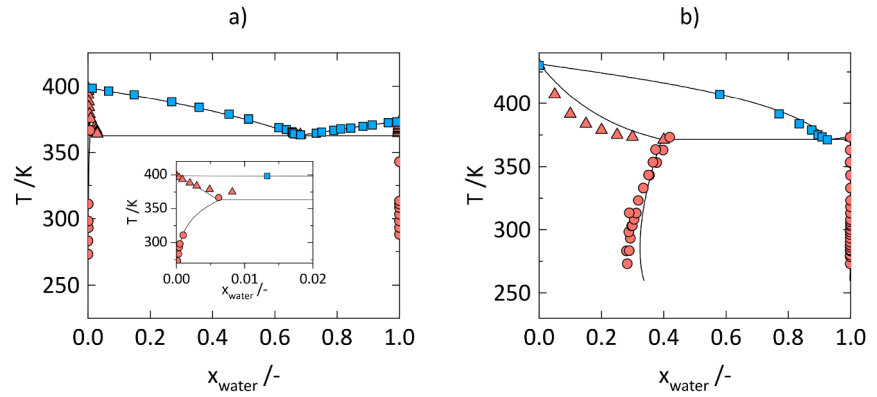

Fig. 12. Phase diagrams (LLE and VLE) of (a) water/n-octane and (b) water/n-hexanol at atmospheric pressure. Squares and triangles are dew points and boiling points, respectively [88,89]. Circles are solubilities [83,84]. Solid lines are results using the hetero-segmented approach.

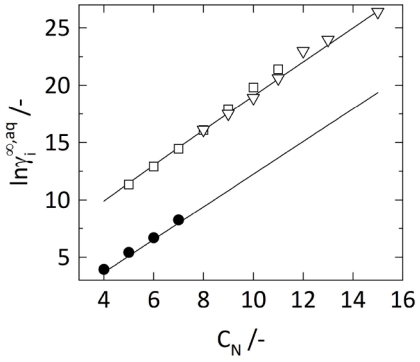

Fig. 13. Activity coefficients of n-alkanes and n-alcohols at infinite dilution in water as a function of carbon number at 298.15 K. n-alkanes are represented as squares [83] and triangles [87]. n-alcohols are represented by circles [90]. Solid lines are predictions using the hetero-segmented approach.

and n-alcohols, which is consistent with a large number of works dedicated to this topic [8,91,92].

Yet, another quantity that describes the infinite-dilution regime is the Henry constant. Fig. 14 presents predicted and experimental values for n-alkanes and n-alcohols in water as functions of carbon number at a temperature of 298.15 K. As can be seen, the new modeling approach is in quantitative agreement with the experimental data, for both the n-alkanes and n-alcohols. As expressed by the data, the n-alkanes are orders of magnitude more volatile than the n-alcohols, reflecting their aversion to be dispersed in water. Contrary, the n-alcohols exhibit small Henry constants, testifying the strong interactions through cross-association. Impressively, this is captured by our GC model in a quantitative and fully predictive manner. Again, both the n-alkanes and the n-alcohols feature a linear dependence of this property with respect to the carbon number.

Eventually, the model performance was validated using octanol/water partition coefficients K_{OW}, as they are the result of complex intermolecular interactions [93]. Furthermore, these data enabled us to assess the model performance for multicomponent mixtures. Fig. 15 shows the comparison of experimental and predicted partition coefficients K_{OW} for the families of n-alkanes and n-alcohols as functions of chain length at a temperature of 298.15 K.

Again, very good agreement with the experimental data is noted. The prediction shows strict linearity and parallelism, consistent with the literature and often exploited for empirical correlations [94–96]. Deteriorations are present for the longer n-alkanes. However, these data come with high uncertainty due to the uncertainty of measuring extremely low solubilities, which is indicated by the large error bars.

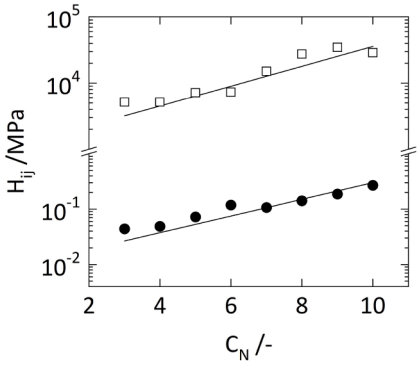

Fig. 14. Henry constants for the n-alkanes and n-alcohols in water as functions of carbon number at 298.15 K. Squares denote data for n-alkanes and circles denote n-alcohols [49]. Solid lines are the predictions using the new modeling approach.

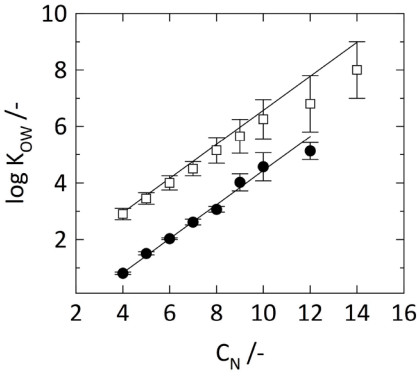

Fig. 15. Octanol/water partition coefficients for the n-alkanes and n-alcohols as functions of carbon number at 298.15 K. Squares for the n-alkanes and circles for the n-alcohols. The experimental data are from ref [93]. Solid lines are predictions using the hetero-segmented approach.

Since the infinite-dilution activity coefficient of a hydrophobic component is known to behave linearly with respect to the carbon number (compare Eq. (9) and Fig. 13)), there is no reason that the partition coefficient should not be linear with respect to the carbon number. Therefore, we can conclude that the model is self-consistent and the approach to describe the hydrophobic interactions generalizes for multicomponent systems.

5. Conclusion

This work extended the parameterization of a hetero-segmented GC approach based on the PC-SAFT framework with special focus on aqueous mixtures subject to the hydrophobic effect. The modeling approach is based on defining distinct functional groups to describe n-alkanes and n-alcohols. For this purpose, we parameterized the CH_2, CH_3, and CH_2OH groups.

The pure-group parameters and group interaction parameters were determined by fitting vapor pressures and saturated-liquid densities of the n-alkanes and n-alcohols. Additional equilibrium data of the n-heptane/n-pentanol mixture completed the data set used for regression. The so-obtained group parameters allow describing the experimental data with an average relative deviation below 2 % and a maximum relative deviation below 5 %. The modeling approach was then validated by predicting properties not used for regression (pure-component properties and VLE/ SLE data of n-alkane/n-alcohol mixtures) with excellent results. In terms of extrapolation capabilities and parameter efficiency, the hetero-segmented approach outperforms the well-established homo-segmented approach of PC-SAFT.

Based on this parametrization, this work established a novel approach to account for the hydrophobic effect, which improves the description of aqueous mixtures containing hydrophobic molecules. The interaction parameters between CH_2, CH_3, and CH_2OH groups on the one hand and water on the other hand were adapted to data on mutual solubilities in n-alkane/water mixtures and in n-alcohol/water mixtures. For all binary mixtures, the concentrations in the two phases were described with an average relative deviation below 6 %. In particular, the solubility minimum of the hydrophobic component in water as a function of temperature was described in excellent agreement with the experimental data. Moreover, the new approach was able to consistently and accurately predict thermodynamic properties such as VLEs and infinite-dilution properties over a wide range of conditions.

In comparison with the literature, the new modeling approach highlights itself by simultaneously and quantitatively describing all phases of aqueous solutions containing n-alkanes and n-alcohols equally well. It is worth noting, that only binary interaction parameters were fitted to obtain these results, while (in contrast to previous works in

literature) the parameters for the different groups, including water, were determined by fitting pure-component data only. This was only possible as hydrophobic interactions were adequately considered by the proposed modeling approach.

Concluding, the new modeling approach proofed its capability in capturing the complex phase behavior of aqueous solutions subject to the hydrophobic effect. This particularly qualifies this modeling approach to describe the behavior of even more complex molecules in aqueous environment as will be shown in the second part of this paper series.

CRediT authorship contribution statement

Marius Rother: Writing – original draft. **Gabriele Sadowski:** Writing – original draft.

Declaration of competing interest

The authors declare that they have no known competing financial interests or personal relationships that could have appeared to influence the work reported in this paper.

Data availability

All data are referenced in the manuscript.

Acknowledgments

The PC-SAFT calculations shown in this work were carried out using the software Solcalc. The Solcalc license was provided by amofor GmbH, Dortmund, Germany.

Appendix

The data on LLE of binary water/n-alkane and water/n-alcohol systems were generated using correlation functions proposed by Mączyński et al. [83], Góral et al. [84] and Tsonopoulos [5]. They are defined as follows

$$\ln x^{aq}_{alkane/alcohol} = a_1 + b_1\left[\frac{c_1}{T} - \ln\frac{c_1}{T} - 1\right] + d_1 exp\left[e_1\left(1 - \frac{T}{f_1}\right)\right] \tag{20}$$

$$\ln x^{org}_{water} = a_2 + b_2 \ln T + \frac{c_2}{T} \tag{21}$$

The aqueous solubility of the n-alkane or n-alcohol is given as $x^{aq}_{alkane/alcohol}$. x^{org}_{water} is the solubility of water in the organic phase. The parameters for Eq. (20) and Eq. (21) are given in Tables 4 and 5, respectively. These parameters were either adapted from literature or determined within this work using available solubility data [41,83–86].

Table 4
Parameters used for correlating solubility data of the n-alkane/n-alcohol in the aqueous phase in n-alkane/water and n-alcohols/water mixtures using Eq. (20).

Component	$a_1/-$	$b_1/-$	c_1/K	$d_1/-$	$e_1/-$	f_1/K	Ref.
n-pentane	−11.482	38.886	311.88	0	0	0	this work
n-hexane	−13.028	47.307	310.60	0	0	0	this work
n-heptane	−14.574	55.728	309.32	0	0	0	this work
n-octane	−16.120	64.149	308.03	0	0	0	this work
n-pentanol	−5.5800	29.700	330.00	1.2990	−20.000	459.80	[77]
n-hexanol	−6.9400	32.900	319.30	0.71300	−20.000	490.50	[77]
n-heptanol	−8.3100	37.100	311.10	0.44000	−40.000	517.70	[77]
n-octanol	−9.6700	41.300	304.50	1.2390	−50.000	545.00	[77]

Table 5
Parameters used for correlating solubility data of water in the organic phase in n-alkane/water and n-alcohols/water mixtures using Eq. (21).

Component	$a_2/-$	$b_2/-$	c_2/K	Ref.
n-pentane	7.1523	0	−4430.7	this work
n-hexane	6.8542	0	−4328.2	this work
n-heptane	6.5561	0	−4225.6	this work
n-octane	6.2580	0	−4123.1	this work
n-pentanol	−39.875	5.8961	1563.7	this work
n-hexanol	−39.997	5.8839	1575.4	this work
n-heptanol	−40.051	5.8717	1587.0	this work
n-octanol	−40.078	5.8595	1598.7	this work

The dispersive BIPs between n-alkanes and n-alcohols for homo-segmented PC-SAFT determined in this work are listed in Table 6. The BIP for n-alkanes and n-alcohols with water used in the homo-segmented approach are listed in Table 7.

Table 6
Interaction parameters for homo-segmented PC-SAFT between the n-alkanes and n-alcohols determined in this work.

Component 1	Component 2	$k_{ij,0}/-$
n-butanol	n-pentane	0.006778
n-butanol	n-hexane	0.01611
n-butanol	n-octane	0.02188
n-butanol	n-decane	0.01511
n-pentanol	n-hexane	0.01484
n-pentanol	n-heptane	0.01482
n-hexanol	n-hexane	0.002975
n-hexanol	n-heptane	0.01012
n-octanol	n-decane	0.01654
n-pentanol	n-pentane	0.005504
n-octanol	n-octane	0.01248
n-octanol	n-dodecane	0.01788
n-octanol	n-undecane	0.01721

Table 7
Interaction parameters for homo-segmented PC-SAFT between the n-alkanes and n-alcohols with water. $\boldsymbol{k_{ij,0}}$, $\boldsymbol{k_{ij,1}}$, $\boldsymbol{k_{ij,2}}$ and $\boldsymbol{k_{ij,3}}$ compute the dispersive BIP $\boldsymbol{k_{ij}}$ as a function of temperature ($\boldsymbol{k_{ij}} = \boldsymbol{k_{ij,0}} + \boldsymbol{k_{ij,1}}/\boldsymbol{T} + \boldsymbol{k_{ij,2}}\ \boldsymbol{T} + \boldsymbol{k_{ij,2}}\ \boldsymbol{T}^2$). $\boldsymbol{l_{ij}^{HB}}$ determines the cross-association strength (compare Eqs. (15), (16), and (17)).

Component	$k_{ij,0}/-$	$k_{ij,1}/K$	$k_{ij,2}/10^{-3}K^{-1}$	$k_{ij,3}/10^{-6}K^{-2}$	$l_{ij}^{HB}/10^{-3}$	Ref.
n-pentane	−0.3054	0	2.419	−2.809	0	[12]
n-hexane	−0.3119	0	2.493	−2.910	0	[12]
n-heptane	−0.3196	0	2.549	−2.993	0	[12]
n-octane	−0.3291	0	2.641	−3.113	0	[12]
n-butanol	0.2660	−43.82	0	0	28.06	this work
n-pentanol	0.2288	−35.91	0	0	23.50	this work
n-hexanol	0.2691	−39.39	0	0	18.09	this work
n-heptanol	0.2534	−37.00	0	0	10.67	this work
n-octanol	0.2802	−39.31	0	0	15.71	this work
n-nonanol	0.2892	−39.78	0	0	13.85	this work

References

[1] L.F. Vega, F. Llovell, Review and new insights into the application of molecular-based equations of state to water and aqueous solutions, in: Fluid Phase Equilib., 416, 2016, pp. 150–173, https://doi.org/10.1016/j.fluid.2016.01.024.

[2] C. Tanford, The Hydrophobic Effect. Formation of Micelles and Biological Membranes, 2. ed., Repr, Wiley, Malabar, Fla, 1991.

[3] S. Garde, G. Hummer, M.E. Paulaitis, Hydrophobic interactions: conformational equilibria and the association of non-polar molecules in water, Faraday Disc. 103 (1996) 125, https://doi.org/10.1039/FD9960300125.

[4] Q. Sun, The Hydrophobic Effects: our Current Understanding, Molecules 27 (2022), https://doi.org/10.3390/molecules27207009.

[5] C. Tsonopoulos, Thermodynamic analysis of the mutual solubilities of normal alkanes and water, Fluid Phase Equilib. 156 (1999) 21–33, https://doi.org/10.1016/S0378-3812(99)00021-7.

[6] F. Biedermann, W.M. Nau, H.-J. Schneider, Neues zum hydrophoben Effekt - Studien mit supramolekularen Komplexen zeigen hochenergetisches Wasser als nichtkovalente Bindungstriebkraft, Angew. Chem. 126 (2014) 11338–11352, https://doi.org/10.1002/ange.201310958.

[7] N.T. Southall, K.A. Dill, A.D.J. Haymet, A view of the hydrophobic effect, J. Phys. Chem. B 106 (2002) 521–533, https://doi.org/10.1021/jp015514e.

[8] J.A. Reynolds, D.B. Gilbert, C. Tanford, Empirical correlation between hydrophobic free energy and aqueous cavity surface area, Proc. Natl. Acad. Sci. U.S.A. 71 (1974) 2925–2927, https://doi.org/10.1073/pnas.71.8.2925.

[9] C. Tsonopoulos, J.L. Heidman, High-pressure vapor-liquid equilibria with cubic equations of state, Fluid Phase Equilib. 29 (1986) 391–414, https://doi.org/10.1016/0378-3812(86)85039-7.

[10] V.N. Kabadi, R.P. Danner, A modified Soave-Redlich-Kwong equation of state for water-hydrocarbon phase equilibria, Ind. Eng. Chem. Proc. Des. Dev. 24 (1985) 537–541, https://doi.org/10.1021/i200030a004.

[11] S. Michel, H.H. Hooper, J.M. Prausnitz, Mutual solubilities of water and hydrocarbons from an equation of state. Need for an unconventional mixing rule, Fluid Phase Equilib. 45 (1989) 173–189, https://doi.org/10.1016/0378-3812(89)80256-0.

[12] N. Haarmann, S. Enders, G. Sadowski, Modeling binary mixtures of n-alkanes and water using PC-SAFT, Fluid Phase Equilib. 470 (2018) 203–211, https://doi.org/10.1016/j.fluid.2017.11.015.

[13] J. Gross, G. Sadowski, Perturbed-chain SAFT: an equation of state based on a perturbation theory for chain molecules, Ind. Eng. Chem. Res. 40 (2001) 1244–1260, https://doi.org/10.1021/ie0003887.

[14] J. Gross, G. Sadowski, Application of the perturbed-chain SAFT equation of state to associating systems, Ind. Eng. Chem. Res. 41 (2002) 5510–5515, https://doi.org/10.1021/ie010954d.

[15] S. Ahmed, N. Ferrando, J.-C. de Hemptinne, J.-P. Simonin, O. Bernard, O. Baudouin, A new PC-SAFT model for pure water, water–hydrocarbons, and water–oxygenates systems and subsequent modeling of VLE, VLLE, and LLE, J. Chem. Eng. Data 61 (2016) 4178–4190, https://doi.org/10.1021/acs.jced.6b00565.

[16] P. Hutacharoen, S. Dufal, V. Papaioannou, R.M. Shanker, C.S. Adjiman, G. Jackson, A. Galindo, Predicting the solvation of organic compounds in aqueous environments: from alkanes and alcohols to pharmaceuticals, Ind. Eng. Chem. Res. 56 (2017) 10856–10876, https://doi.org/10.1021/acs.iecr.7b00899.

[17] D. NguyenHuynh, Accurate modeling of multiphase behavior of aqueous systems. I. Alkanes, alkenes, cycloalkanes, alcohols, aromatics, Fluid Phase Equilib. 473 (2018) 201–219, https://doi.org/10.1016/j.fluid.2018.06.019.

[18] S. Tamouza, J.-P. Passarello, P. Tobaly, J.-C. de Hemptinne, Group contribution method with SAFT EOS applied to vapor liquid equilibria of various hydrocarbon series, Fluid Phase Equilib. 222-223 (2004) 67–76, https://doi.org/10.1016/j.fluid.2004.06.038.

[19] S. Tamouza, J.-P. Passarello, P. Tobaly, J.-C. de Hemptinne, Application to binary mixtures of a group contribution SAFT EOS (GC-SAFT), Fluid Phase Equilib. 228-229 (2005) 409–419, https://doi.org/10.1016/j.fluid.2004.10.003.

[20] T.X. Nguyen Thi, S. Tamouza, P. Tobaly, J.-P. Passarello, J.-C. de Hemptinne, Application of group contribution SAFT equation of state (GC-SAFT) to model phase behaviour of light and heavy esters, Fluid Phase Equilib. 238 (2005) 254–261, https://doi.org/10.1016/j.fluid.2005.10.009.

[21] D. NguyenHuynh, J.-P. Passarello, P. Tobaly, J.-C. de Hemptinne, Application of GC-SAFT EOS to polar systems using a segment approach, Fluid Phase Equilib. 264 (2008) 62–75, https://doi.org/10.1016/j.fluid.2007.10.019.

[22] D. Nguyen-Huynh, J.-P. Passarello, P. Tobaly, J.-C. de Hemptinne, Modeling phase equilibria of asymmetric mixtures using a group-contribution SAFT (GC-SAFT) with a kij correlation method based on London's theory. 1. Application to CO_2 + n -alkane, methane + n -alkane, and ethane + n -alkane systems, Ind. Eng. Chem. Res. 47 (2008) 8847–8858, https://doi.org/10.1021/ie071643r.

[23] D. Nguyen-Huynh, T.K.S. Tran, S. Tamouza, J.-P. Passarello, P. Tobaly, J.-C. de Hemptinne, Modeling phase equilibria of asymmetric mixtures using a group-contribution SAFT (GC-SAFT) with a kij correlation method based on London's theory. 2. Application to binary mixtures containing aromatic hydrocarbons, n -alkanes, CO_2, N_2, and H_2S, Ind. Eng. Chem. Res. 47 (2008) 8859–8868, https://doi.org/10.1021/ie071644j.

[24] N. Haarmann, S. Enders, G. Sadowski, Heterosegmental modeling of long-chain molecules and related mixtures using PC-SAFT: 2. Associating compounds, Ind. Eng. Chem. Res. 58 (2019) 4625–4643, https://doi.org/10.1021/acs.iecr.9b00157.
[25] S.P. Tan, J.S. Kargel, S.D. Vance, R.M. Lopes, Modeling binary mixtures of water + light hydrocarbon using the perturbed-chain statistical associating fluid theory with induced association: improvement in describing all equilibrium phases, ACS Earth Space Chem. 3 (2019) 2569–2581, https://doi.org/10.1021/acsearthspacechem.9b00229.
[26] D. Asthagiri, A. Valiya Parambathu, D. Ballal, W.G. Chapman, Electrostatic and induction effects in the solubility of water in alkanes, J. Chem. Phys. 147 (2017) 74506, https://doi.org/10.1063/1.4997916.
[27] D. Ballal, P. Venkataraman, W.A. Fouad, K.R. Cox, W.G. Chapman, Isolating the non-polar contributions to the intermolecular potential for water-alkane interactions, J. Chem. Phys. 141 (2014) 64905, https://doi.org/10.1063/1.4892341.
[28] J.G. McDaniel, A. Yethiraj, Comment on "Isolating the non-polar contributions to the intermolecular potential for water-alkane interactions", J. Chem. Phys. 141, 064905 (2014), J. Chem. Phys. 144 (2016) 137101, https://doi.org/10.1063/1.4944978.
[29] D. Asthagiri, D. Ballal, P. Venkataraman, W.A. Fouad, K.R. Cox, W.G. Chapman, Response to, Comment on 'Isolating the non-polar contributions to the intermolecular potential for water-alkane interactions, J. Chem. Phys. 144, 137101 (2016), J. Chem. Phys. 144 (2016) 137102, https://doi.org/10.1063/1.4944979.
[30] M. Kleiner, G. Sadowski, Modeling of polar systems using PCP-SAFT: an approach to account for induced-association interactions, J. Phys. Chem. C 111 (2007) 15544–15553, https://doi.org/10.1021/jp072640v.
[31] N. Haarmann, S. Enders, G. Sadowski, Heterosegmental modeling of long-chain molecules and related mixtures using PC-SAFT: 1. Polar compounds, Ind. Eng. Chem. Res. 58 (2019) 2551–2574, https://doi.org/10.1021/acs.iecr.8b03799.
[32] J.M. Prausnitz, R.N. Lichtenthaler, E.G. de Azevedo, Molecular Thermodynamics of Fluid-Phase equilibria, 3. Ed.,Prentice-Hall International Series in the Physical and Chemical Engineering Sciences, Prentice-Hall PTR, Upper Saddle River, NJ, 1999.
[33] W.G. Chapman, K.E. Gubbins, G. Jackson, M. Radosz, SAFT: equation-of-state solution model for associating fluids, Fluid Phase Equilib. 52 (1989) 31–38, https://doi.org/10.1016/0378-3812(89)80308-5.
[34] C. Held, T. Reschke, S. Mohammad, A. Luza, G. Sadowski, ePC-SAFT revised, Chem. Eng. Res. Design 92 (2014) 2884–2897, https://doi.org/10.1016/j.cherd.2014.05.017.
[35] J. Gross, O. Spuhl, F. Tumakaka, G. Sadowski, Modeling copolymer systems using the perturbed-chain SAFT equation of state, Ind. Eng. Chem. Res. 42 (2003) 1266–1274, https://doi.org/10.1021/ie020509y.
[36] T.-B. Nguyen, J.-C. de Hemptinne, B. Creton, G.M. Kontogeorgis, Improving GC-PPC-SAFT equation of state for LLE of hydrocarbons and oxygenated compounds with water, Fluid Phase Equilib. 372 (2014) 113–125, https://doi.org/10.1016/j.fluid.2014.03.028.
[37] A.J. Haslam, A. Galindo, G. Jackson, Prediction of binary intermolecular potential parameters for use in modelling fluid mixtures, Fluid Phase Equilib. 266 (2008) 105–128, https://doi.org/10.1016/j.fluid.2008.02.004.
[38] W.G. Chapman, G. Jackson, K.E. Gubbins, Phase equilibria of associating fluids, Mol. Phys. 65 (1988) 1057–1079, https://doi.org/10.1080/00268978800101601.
[39] J.P. Wolbach, S.I. Sandler, Using molecular orbital calculations to describe the phase behavior of cross-associating mixtures, Ind. Eng. Chem. Res. 37 (1998) 2917–2928, https://doi.org/10.1021/ie9707811.
[40] G.M. Kontogeorgis, G.K. Folas, Thermodynamic Models for Industrial Applications, John Wiley & Sons, Ltd, Chichester, UK, 2010.
[41] P. Morgado, J. Barras, P. Duarte, E.J. Filipe, Solubility of water in n-alkanes: new experimental measurements and molecular dynamics simulations, Fluid Phase Equilib. 503 (2020) 112322, https://doi.org/10.1016/j.fluid.2019.112322.
[42] S. Lüdemann, R. Abseher, H. Schreiber, O. Steinhauser, The temperature-dependence of hydrophobic association in water. Pair versus bulk hydrophobic interactions, J. Am. Chem. Soc. 119 (1997) 4206–4213, https://doi.org/10.1021/ja953439d.
[43] S. Lüdemann, H. Schreiber, R. Abseher, O. Steinhauser, The influence of temperature on pairwise hydrophobic interactions of methane-like particles: a molecular dynamics study of free energy, J. Chem. Phys. 104 (1996) 286–295, https://doi.org/10.1063/1.470899.
[44] Q. Sun, Y. Fu, W. Wang, Temperature effects on hydrophobic interactions: implications for protein unfolding, Chem. Phys. 559 (2022) 111550, https://doi.org/10.1016/j.chemphys.2022.111550.
[45] S.R. Durell, A. Ben-Naim, Temperature dependence of hydrophobic and hydrophilic forces and interactions, J. Phys. Chem. B 125 (2021) 13137–13146, https://doi.org/10.1021/acs.jpcb.1c07802.
[46] K. Kiesow, F. Tumakaka, G. Sadowski, Experimental investigation and prediction of oiling out during crystallization process, J. Cryst. Growth 310 (2008) 4163–4168, https://doi.org/10.1016/j.jcrysgro.2008.06.034.
[47] X. Liang, I. Tsivintzelis, G.M. Kontogeorgis, Modeling water containing systems with the simplified PC-SAFT and CPA equations of state, Ind. Eng. Chem. Res. 53 (2014) 14493–14507, https://doi.org/10.1021/ie501993y.
[48] I. Goodfellow, Y. Bengio, A. Courville, Deep Learning, Adaptive Computation and Machine Learning, The MIT Press, Cambridge, Massachusetts, London, England, 2016.
[49] C.L. Yaws, The Yaws Handbook of Thermodynamic Properties for Hydrocarbons and Chemicals. Heat Capacities, Enthalpies of Formation, Gibbs Energies of Formation, Entropies, and other Thermodynamic Properties; Gases, Liquids, and Solids; Coverage for more than 12,800 Organic and Inorganic Chemicals; C1 to C100 Organics and Ac to Zr Inorganics, Gulf Publishing Company, Houston, Tex., 2006.
[50] J. Vijande, M.M. Piñeiro, J.L. Legido, Group-contribution method with proximity effect for PC-SAFT molecular parameters. 2. Application to association parameters: primary alcohols and amines, Ind. Eng. Chem. Res. 53 (2014) 909–919, https://doi.org/10.1021/ie4023786.
[51] V. Papaioannou, T. Lafitte, C. Avendaño, C.S. Adjiman, G. Jackson, E.A. Müller, A. Galindo, Group contribution methodology based on the statistical associating fluid theory for heteronuclear molecules formed from Mie segments, J. Chem. Phys. 140 (2014) 54107, https://doi.org/10.1063/1.4851455.
[52] A. Chremos, E. Forte, V. Papaioannou, A. Galindo, G. Jackson, C.S. Adjiman, Modelling the phase and chemical equilibria of aqueous solutions of alkanolamines and carbon dioxide using the SAFT-γ SW group contribution approach, Fluid Phase Equilib. 407 (2016) 280–297, https://doi.org/10.1016/j.fluid.2015.07.052.
[53] M. Mohsen-Nia, M.R. Memarzadeh, Isobaric vapor−liquid equilibria of heptane + 1-butanol and heptane + 1-pentanol systems at (53.3 and 91.3) kPa, J. Chem. Eng. Data 55 (2010) 2140–2144, https://doi.org/10.1021/je9006629.
[54] J. Gross, G. Sadowski, Modeling polymer systems using the perturbed-chain statistical associating fluid theory equation of state, Ind. Eng. Chem. Res. 41 (2002) 1084–1093, https://doi.org/10.1021/ie010449g.
[55] K. Albers, M. Heilig, G. Sadowski, Reducing the amount of PCP–SAFT fitting parameters. 2. Associating components, Fluid Phase Equilib. 326 (2012) 31–44, https://doi.org/10.1016/j.fluid.2012.04.014.
[56] R. Todeschini, V. Consonni, Handbook of Molecular Descriptors, 1. Auflage. Methods and Principles in Medicinal Chemistry 11, Wiley-VCH, Weinheim, 2008.
[57] Y.H. Zhao, M.H. Abraham, A.M. Zissimos, Fast calculation of van der Waals volume as a sum of atomic and bond contributions and its application to drug compounds, J. Org. Chem. 68 (2003) 7368–7373, https://doi.org/10.1021/jo034808o.
[58] V. Consonni, R. Todeschini, M. Pavan, Structure/response correlations and similarity/diversity analysis by GETAWAY descriptors. 1. Theory of the novel 3D molecular descriptors, J. Chem. Inf. Comput. Sci. 42 (2002) 682–692, https://doi.org/10.1021/ci015504a.
[59] G.C. Pimentel, A.L. McClellan, The Hydrogen Bond, W.H. Freeman, San Francisco, 1960.
[60] C. Zhu, X. Liu, M. He, G.M. Kontogeorgis, X. Liang, Heat capacities of fluids: the performance of various equations of state, J. Chem. Eng. Data 65 (2020) 5654–5676, https://doi.org/10.1021/acs.jced.0c00649.
[61] R. Páramo, M. Zouine, C. Casanova, New batch cells adapted to measure saturated heat capacities of liquids, J. Chem. Eng. Data 47 (2002) 441–448, https://doi.org/10.1021/je0155103.
[62] J.C. van Miltenburg, H. Gabrielová, K. Růžička, Heat capacities and derived thermodynamic functions of 1-hexanol, 1-heptanol, 1-octanol, and 1-decanol between 5K and 390K, J. Chem. Eng. Data 48 (2003) 1323–1331, https://doi.org/10.1021/je0340856.
[63] M. Davies, B. Kybett, Sublimation and vaporization heats of long-chain alcohols, Trans. Faraday Soc. 61 (1965) 1608, https://doi.org/10.1039/TF9656101608.
[64] G. Nichols, S. Kweskin, M. Frericks, S. Reiter, G. Wang, J. Orf, B. Carvallo, D. Hillesheim, J. Chickos, Evaluation of the vaporization, fusion, and sublimation enthalpies of the 1-alkanols: the vaporization enthalpy of 1-, 6-, 7-, and 9-heptadecanol, 1-octadecanol, 1-eicosanol, 1-docosanol, 1-hexacosanol, and cholesterol at T = 298.15K by correlation gas chromatography, J. Chem. Eng. Data 51 (2006) 475–482, https://doi.org/10.1021/je0503857.
[65] V. Piacente, T. Pompili, P. Scardala, D. Ferro, Temperature dependence of the vaporization enthalpies of n-alkanes from vapour-pressure measurements, J. Chem. Thermodyn. 23 (1991) 379–396, https://doi.org/10.1016/S0021-9614(05)80092-8.
[66] R.D. Chirico, an Nguyen, W.V. Steele, M.M. Strube, C. Tsonopoulos, The vapor pressure of n-alkanes revisited. New high-precision vapor pressure data on n-decane, n-eicosane, and n-octacosane, J. Chem. Eng. Data 34 (1989) 149–156, https://doi.org/10.1021/je00056a002.
[67] Y. Kim, W. Bae, H. Kim, Isothermal vapor−liquid equilibria for the n -pentane + 1-butanol and n -pentane + 2-butanol systems near the critical region of the mixtures, J. Chem. Eng. Data 50 (2005) 1520–1524, https://doi.org/10.1021/je049894j.
[68] M. Dominguez, A.M. Mainar, H. Artigas, F.M. Royo, J.S. Urieta, Isobaric VLE data of the ternary system (1-Butanol+n-Hexane+1-Butylamine) and the three constituent binary mixtures at 101.3kPa, J. Chem. Eng. Japan /JCEJ 30 (1997) 484–490, https://doi.org/10.1252/JCEJ.30.484.
[69] T. Hiaki, A. Taniguchi, T. Tsuji, M. Hongo, K. Kojima, Isobaric vapor−liquid equilibria of octane + 1-butanol, +2-butanol, and +2-methyl-2-propanol at 101.3kPa, J. Chem. Eng. Data 41 (1996) 1087–1090, https://doi.org/10.1021/JE960112Z.
[70] S. Bernatová, J. Linek, I. Wichterle, Vapour-liquid equilibrium in the butyl alcohol -n-decane system at 85, 100 and 115°C, Fluid Phase Equilib. 74 (1992) 127–132, https://doi.org/10.1016/0378-3812(92)85057-F.
[71] M. Ronc, G.R. Ratcliff, Measurement of vapor-liquid equilibria using a semi-continuous total pressure static equilibrium still, Can. J. Chem. Eng. 54 (1976) 326–332, https://doi.org/10.1002/cjce.5450540414.
[72] S.H. Du Plessis, S.A.M. Smith, C. Latsky-Galloway, C.E. Schwarz, Investigation of the low-pressure phase behavior and SAFT modeling of 1-alcohol and n -alkane binary systems, J. Chem. Eng. Data 68 (2023) 2898–2912, https://doi.org/10.1021/acs.jced.3c00346.
[73] I. Máchová, J. Linek, I. Wichterle, Vapour—Liquid equilibria in the heptane - 1-pentanol and heptane - 3-methyl-1-butanol systems at 75, 85 and 95°C, Fluid Phase Equilib. 41 (1988) 257–267, https://doi.org/10.1016/0378-3812(88)80010-4.

[74] P.R. Rao, C. Chiranjivi, C.J. Dasarao, Vapour-liquid equilibria systems: hexane-hexylalcohol and heptane-hexylalcohol, J. Appl. Chem. 18 (1968) 166–168, https://doi.org/10.1002/jctb.5010180602.
[75] Z. Plesnar, P. Gierycz, A. Bylicki, Vapour-liquid equilibrium and solid-liquid equilibrium in the system formed by 1-octanol and n-octane, Thermochim. Acta 128 (1988) 93–98, https://doi.org/10.1016/0040-6031(88)85355-3.
[76] S.H. Du Plessis, C. Latsky-Galloway, C.E. Schwarz, Low-pressure phase equilibrium data for binary systems of 1-alcohols (C n OH) and n -alkanes (C n +2), J. Chem. Eng. Data (2023), https://doi.org/10.1021/acs.jced.3c00026.
[77] M. Góral, P. Oracz, A. Skrzecz, A. Bok, A. Mączyński, Recommended vapor–liquid equilibrium data. Part 1: binary n -alkanol– n -alkane systems, J. Phys. Chem. Ref. Data 31 (2002) 701–748, https://doi.org/10.1063/1.1480097.
[78] Z. Plesnar, P. Gierycz, A. Bylicki, Solid + liquid) equilibria in (butan-1-ol + n-decane or n-octane), J. Chem. Thermodyn. 22 (1990) 403–406, https://doi.org/10.1016/0021-9614(90)90128-D.
[79] Z. Plesnar, P. Gierycz, J. Gregorowicz, A. Bylicki, Vapour-liquid equilibrium and solid-solid equilibrium in the system formed by octan-1-ol and n-decane: measurement and calculation, Thermochim. Acta 150 (1989) 101–109, https://doi.org/10.1016/0040-6031(89)85316-X.
[80] Z. Plesnar, P. Gierycz, A. Bylicki, Solid + liquid) equilibria in (n-octan-1-ol + n-hexadecane or n-dodecane or n-undecane), J. Chem. Thermodyn. 22 (1990) 393–398, https://doi.org/10.1016/0021-9614(90)90126-B.
[81] S.G. Collins, J.J. Christensen, R.M. Izatt, R.W. Hanks, The excess enthalpies of 10 (n-pentane + an n-alkanol) mixtures at 298.15K, J. Chem. Thermodyn. 12 (1980) 609–614, https://doi.org/10.1016/0021-9614(80)90081-6.
[82] E. Mascato, L. Mussari, M. Postigo, A.B. Mariano, M.M. Piñeiro, J.L. Legido, M. I. Paz Andrade, Excess enthalpy, density, and speed of sound for the ternary mixture methyl tert -butyl ether (1) + butan-1-ol (2) + octane (3), J. Chem. Eng. Data 54 (2009) 453–458, https://doi.org/10.1021/je8004613.
[83] A. Mączyński, B. Wiśniewska-Gocłowska, M. Góral, Recommended liquid–liquid equilibrium data. Part 1. Binary alkane–water systems, J. Phys. Chem. Ref. Data 33 (2004) 549–577, https://doi.org/10.1063/1.1643922.
[84] M. Góral, B. Wiśniewska-Gocłowska, A. Mączyński, Recommended liquid–liquid equilibrium data. Part 4. 1-alkanol–water systems, J. Phys. Chem. Ref. Data 35 (2006) 1391–1414, https://doi.org/10.1063/1.2203354.
[85] M.G. Freire, L. Gomes, L.M.N.B.F. Santos, I.M. Marrucho, J.A.P. Coutinho, Water solubility in linear fluoroalkanes used in blood substitute formulations, J. Phys. Chem. B 110 (2006) 22923–22929, https://doi.org/10.1021/jp0622942.
[86] B.E. Lang, Solubility of water in octan-1-ol from (275 to 369) K, J. Chem. Eng. Data 57 (2012) 2221–2226, https://doi.org/10.1021/je3001427.
[87] J. Tolls, J. van Dijk, E.J.M. Verbruggen, J.L.M. Hermens, B. Loeprecht, G. Schüürmann, Aqueous solubility−molecular size relationships: a mechanistic case study using C 10 - to C 19 -alkanes, J. Phys. Chem. A 106 (2002) 2760–2765, https://doi.org/10.1021/jp011755a.
[88] M. Tu, D. Fei, Y. Liu, J. Wang, Phase equilibrium for partially miscible system of octane - water, Chin. J. Chem. Eng. 12 (1998) 325–330.
[89] S.P. Tunik, T.M. Lesteva, Chernaya, Phase equilibria in water + alcohols + formaldehyde systems: I. the liquid- vapor equilibria in the systems water + c(6) and c(7) alcohols, Russ. J. Phys. Chem. A 51 (1977) 751.
[90] K. Kojima, S. Zhang, T. Hiaki, Measuring methods of infinite dilution activity coefficients and a database for systems including water, Fluid Phase Equilib. 131 (1997) 145–179, https://doi.org/10.1016/S0378-3812(96)03210-4.
[91] R.B. Hermann, Theory of hydrophobic bonding. II. Correlation of hydrocarbon solubility in water with solvent cavity surface area, J. Phys. Chem. 76 (1972) 2754–2759, https://doi.org/10.1021/j100663a023.
[92] S.M.J. Harris, T. Higuchi, J.H. Rytting, Thermodynamic group contributions from ion pair extraction equilibriums for use in the prediction of partition coefficients. Correlation of surface area with group contributions, J. Phys. Chem. 77 (1973) 2694–2703, https://doi.org/10.1021/j100640a027.
[93] J. Sangster, Octanol-Water Partition Coefficients. Fundamentals and Physical Chemistry,Wiley Series in Solution Chemistry 2, John Wiley & Sons, Ltd, Chichester, 1997.
[94] P. Ruelle, The n-octanol and n-hexane/water partition coefficient of environmentally relevant chemicals predicted from the mobile order and disorder (MOD) thermodynamics, Chemosphere 40 (2000) 457–512, https://doi.org/10.1016/S0045-6535(99)00268-4.
[95] A.A. Sevastos, C.M. Baker, P. Taylor, A simple method for predicting alkane-water partition coefficients of surfactants, J. Surf. Deterg. 25 (2022) 53–61, https://doi.org/10.1002/jsde.12545.
[96] P. Molyneux, Octanol/water partition coefficients Kow: a critical examination of the value of the methylene group contribution to logKow for homologous series of organic compounds, Fluid Phase Equilib. 368 (2014) 120–141, https://doi.org/10.1016/j.fluid.2014.01.014.